

Neutron Scattering Contrast & Character

The Polarization Separation

Polarization Tutorial

Neutrons are NOT Neutral!

- Why!?! Electrically charged quarks within
- Neutron **spin** affects **weak force** interaction
 - Neutron **magnetic dipole moment** affects **magnetic** interaction

Spin: $\sigma_n = \frac{1}{2}$ $P = 2(\sigma_n)$
 $|P| < 1$

Dipole moment:
 $\mu_n = -1.913 \mu_N$
 Nuclear magneton:
 $\mu_N = 5.051E - 27 \text{ JT}^{-1}$

*Expressions of Coherence

Bragg Scattering & Coherent Inelastic scattering

Size scale: Å - nm

Leverages: lattice periodicity for single crystals or powders & dynamic perturbations

Instruments measuring this: diffractometers, triple axis spectrometers, direct geometry spectrometers

Math of Polarization Separation: Leads to the Maleev-Blume^{1,2} equations for both changes in scattered intensity and changes in neutron polarization state. Relevant terms are scattered throughout tables at right.

Index of refraction

Size scale: nm - μm

Leverages: # density variation

Instruments measuring this: Small angle neutron scattering (SANS) & Reflectometers

Math of Polarization Separation: For e.g. 1D multilayer systems, it's NOT periodic so one must directly solve Schrodinger's equation

Diffuse scattering

Size scale: Å - nm

Leverages: Local structural variations from longer range lattice periodicity

Instruments measuring this: Diffuse scattering elastic instruments like WAND² and CORELLI

Math of Polarization Separation: Maleev-Blume^{1,2} vector equations also used here

Unpolarized perspective / review of neutron scattering contrast and character

Neutron Scattering Contrast

What the neutron interacts with

	Weak Force	Magnetism
Neutron scatters from:	Nuclei of atoms	Magnetism in material
Real space	Highly localized (small nuclei)	Extended via electron orbits & extended field profiles
Reciprocal space (Fourier-transformed space)	Structure factor generally strongest at <u>higher</u> momentum transfer Q	Structure factor generally strongest at <u>lower</u> momentum transfer Q

Neutron Scattering Character

How the neutron interacts

	Incoherent	Coherent*	Absorption
How much of material	Individual atom position or motion	Sets of atoms or moments; collective motion	Individual atom
Scattering 'area' or 'length'	Area / cross section	Length (can be negative or 3D)	Area / cross section
Scatter direction	Mostly isotropic / broad	Very directional (e.g. Bragg peaks)	N/A
Excitation sensitivity	Great for stationary excitations & diffusion	Great for moving excitations with dispersion	N/A

Unpolarized perspective on Contrast / Character Matrix

	Incoherent	Coherent	Absorption
Weak force	Both I_n and I_{si} <ul style="list-style-type: none"> • I_n: Isotope Incoherent Scattering via randomness of same element but different isotopes -or- deconstructive interference of coherent scattering lengths (like TiZr) • I_{si}: Spin Incoherent Scattering via randomness of same isotope but different nuclear spin orientations (like V) 	N : Nuclear coherent scattering structure factor $N(Q) = \sum_n b_n e^{iQ \cdot R_n}$	σ_{abs} differs by isotope
Magnetism	N/A (?)	M : Magnetic coherent scattering $M(Q) = \sum_n M_n e^{iQ \cdot R_n}$	N/A

New Dimension to Contrast / Character Matrix via Spin

Weak force only	Incoherent	Coherent	Absorption
Scattered Intensity	<ul style="list-style-type: none"> • I_n doesn't change • I_{si} can be reduced by co-aligning or anti-aligning nuclear spin with respect to neutron spin via Dynamic Nuclear Polarization (DNP) 	$N^\dagger N$ changes by co-aligning or anti-aligning nuclear spin with respect to neutron spin	σ_{abs} differs by the relative orientation of the neutron spin and the nuclear spin
Changes to neutron spin state	$P I_n$ $-\frac{1}{3} P I_{si}$	$P N^\dagger N$	N/A

New Dimension to Contrast / Character Matrix via Magnetic Moment

$e_Q = Q/ Q $	Incoherent	Coherent	Absorption
Magnetism Only	N/A (?)	Unit vector along momentum transfer Q	$M_\perp = e_Q \times M(Q) \times e_Q$
Scattered Intensity	N/A (?)	Depends on relative orientation of incident neutron polarization P and M_\perp in different ways: <ul style="list-style-type: none"> • Enhanced scatter from Ferromagnet $M_\perp^\dagger M_\perp$ • Chiral magnetic structure $iP \cdot (M_\perp^\dagger \times M_\perp)$ 	N/A
Changes to neutron Magnetic Moment	N/A (?)	Depends on relative orientation of incident neutron polarization P and M_\perp in different ways: <ul style="list-style-type: none"> • "spin flip" or "non-spin-flip": $(P \cdot M_\perp^\dagger) M_\perp + (P \cdot M_\perp) M_\perp^\dagger - P(M_\perp^\dagger M_\perp)$ • Chiral magnetic structure: $iN(P \times M_\perp^\dagger) - iN^\dagger(P \times M_\perp)$ 	N/A

New Dimension to Contrast / Character Matrix via Spin and Magnetic Moment

Both weak force and magnetism	Incoherent	Coherent	Absorption
Scattered Intensity	N/A	Think constructive or destructive interference: $P \cdot M_\perp^\dagger N + P \cdot M_\perp N^\dagger$	N/A
Changes to neutron Magnetic Moment	N/A	Think constructive or destructive interference: $N M_\perp^\dagger + N^\dagger M_\perp$	N/A

Putting it all together...

Scattered Intensity

$$I = I_n + N^\dagger N + I_{si} + M_\perp^\dagger M_\perp + P \cdot M_\perp^\dagger N + P \cdot M_\perp N^\dagger + iP \cdot (M_\perp^\dagger \times M_\perp)$$

Changes to neutron polarization state

$$P' = P \left(I_n + N^\dagger N - \frac{1}{3} I_{si} \right) + (P \cdot M_\perp^\dagger) M_\perp + (P \cdot M_\perp) M_\perp^\dagger - P(M_\perp^\dagger M_\perp) + iN(P \times M_\perp^\dagger) - iN^\dagger(P \times M_\perp) + N M_\perp^\dagger + N^\dagger M_\perp - i(M_\perp^\dagger \times M_\perp)$$

P, P' Initial and final neutron polarization

How saturated components leverage the Contrast / Character Matrix to serve as Polarization Filters

Scattered Intensity Only	Incoherent	Coherent	Absorption
Weak force	Polarized Hydrogen nuclei in e.g. naphthalene is preferentially scattered incoherently for just one neutron spin state		Polarized ³ He nuclei preferentially absorbs neutrons with just one neutron spin state
Magnetism		The magnetic index of refraction differs from unity for one neutron spin state but not the opposite. Both critical internal reflection and supermirror multilayers can leverage this for preferential reflection of one spin state and transmission of the other	
Both weak force and magnetism		The magnetic Bragg peak generates opposite sign scattering length for moment-up vs moment-down scattering. This induces either constructive or destructive interference with nuclear coherent scattering satisfying the same Bragg condition. So, find the appropriate Bragg peak with comparable scattering length magnitudes for magnetic and nuclear scattering, and voila! Some Heusler alloys have nearly identical scattering lengths for particular Bragg peaks.	

Polarization 101 Exercise: - build a “polarization application” statement for your research -

2024

Polarized neutrons enable a variety of capabilities which enhance ‘unpolarized’ neutron scattering techniques by separating different aspects and dimensions of scattering, or by providing high-resolution in energy and/or angle. This poster / handout is intended for prospective users of polarized neutrons, as a workflow to determine whether and how polarized neutrons might help you answer some of your more pressing questions, to navigate the wide range of capabilities, and to help you prepare proposals for experiments. This template approach is utilized in neighboring posters / handouts to provide a consistent framework for understanding the wide range of applications which leverage polarized neutrons, and to clarify which neutron scattering instruments can access which configurations.

STATEMENT TEMPLATE

As a [**SCIENCE AREA**] neutron scattering experimentalist, I want to [**CAPABILITY FAMILY**] when using [**NEUTRON SCATTERING TECHNIQUE**] with [**NEUTRON POLARIZATION CONFIGURATION**] so I can [**APPLICATION statement**] for [**SCIENCE EXAMPLE**]

SCIENCE AREA

- Biology
- Soft matter & Polymers
- Materials & Engineering
- Condensed matter & Quantum materials
- Chemistry / Geology
- Environmental Science

SCIENCE EXAMPLE

- What system(s) or material(s) are you studying right now?

NEUTRON SCATTERING TECHNIQUE

- Imaging
- Reflectometry
- (μ)Small Angle Neutron Scattering
- Diffraction (powder or single crystal)
- Quasielastic Scattering
- Direct Geometry / Triple Axis Spectroscopy
- Indirect Geometry Spectroscopy

Structure
Dynamics

UNPOLARIZED LIMITATION?

- ...with the unpolarized data you've already obtained and are trying to analyze.
- Do you need to separate contributions to the observed scattering?
- Do you need enhanced momentum and / or energy resolution?

CAPABILITY FAMILY

Isolate nuclear scattering	N & I_N
Isolate spin-incoherent scattering	I_{si}
Leverage dynamic nuclear polarization	$N \leftrightarrow I_{si}$
Solve Phase Problem	N & M_{\perp}
Explore magnetic scattering	M_{\perp}
Explore coinciding of nuclear and magnetic scattering	N with M_{\perp}
Explore magnetic chirality	M_{\perp} cross terms
Enhance time / energy resolution	I_N, I_{si}, N & M_{\perp}
Enhance Q / size resolution	N & M_{\perp}
Match resolution to dispersion	N & M_{\perp}

APPLICATION STATEMENT

- Describe how this capability family will remove the unpolarized limitation and help you better understand your science example

$N(Q) = \sum_n b_n e^{iQ \cdot R_n}$	Nuclear structure factor
$M_{\perp} = e_Q \times M(Q) \times e_Q$	“M perpendicular”
$M(Q) = \sum_n M_n e^{iQ \cdot R_n}$	Fourier transform of magnetic moments / magnetic structure factor
$e_Q = Q/ Q $	Unit vector along momentum transfer Q
I_{si}	Spin incoherent scattered intensity
P, P^1	Initial and final polarization

MALEEV-BLUME EQUATIONS ACCESS SCATTERED INTENSITY & CHANGES IN NEUTRON POLARIZATION STATE

$$I = N^{\dagger}N + I_{si} + M_{\perp}^{\dagger}M_{\perp} + P \cdot M_{\perp}^{\dagger}N + P \cdot M_{\perp}N^{\dagger} + iP \cdot (M_{\perp}^{\dagger} \times M_{\perp})$$

$$P^1 I = P \left(I_n + N^{\dagger}N - \frac{1}{3}I_{si} \right) + (P \cdot M_{\perp}^{\dagger})M_{\perp} + (P \cdot M_{\perp})M_{\perp}^{\dagger} - P(M_{\perp}^{\dagger}M_{\perp}) + iN(P \times M_{\perp}^{\dagger}) - iN^{\dagger}(P \times M_{\perp}) + NM_{\perp}^{\dagger} + N^{\dagger}M_{\perp} - i(M_{\perp}^{\dagger} \times M_{\perp})$$

SEPARATE: IDENTIFY RELEVANT TERMS IN M-B EQUATIONS...

- Applications which separate or isolate (spin) incoherent from coherent, or magnetic direction-dependent contributions
- Select one or a few terms in the Maleev-Blume equations which speak to the capability which you intend to leverage
- **Special case #1:** Coalign system nuclei to switch from I_{si} to N
- **Special case #2:** two different M_{\perp} substrates to solve phase problem
- **Special case #3:** $P \parallel P^1$, i.e. change in polarization state is other than just ‘spin flip’ or ‘non-spin-flip’ due to cross terms (chirality and lattice-magnetic interference)

RESOLUTION: IDENTIFY NEEDED ENHANCEMENT

- Applications which enhance resolution (energy, momentum transfer, or some combination) for a given neutron scattering technique (preserves the energy or momentum transfer range)
- **Special case #4:** Evaluation of polarization state is tied to deliberate precession / phasing of neutron polarization state. This manipulation of P & P^1 is not found in the M-B equations
- Larmor precession:

$$\vec{\tau} = \vec{\mu} \times \vec{B}, \omega = -\gamma B$$

TO DETERMINE CONFIGURATION

POLARIZATION CONFIGURATION	Measures the scattered neutron	Optics
Half Polarized Dynamic Nuclear Polarization Solve Phase Problem	Intensity	1 filter 1 flipper
Longitudinal Analysis I Larmor	Polarization State	2 filters 1 flipper
Longitudinal Analysis II Spherical Neutron Polarimetry	Both	2 filters 2 flippers

- Fortunately, most terms in the M-B equations can be safely ignored by accounting for the physics of the system under study
- Becomes a linear / vector algebra problem, with multiple choices for incident (P) and sometimes final (P^1) polarization
- Polarization terminology for different scattering technique / instrument classes has developed independently, so this terminology is not universal

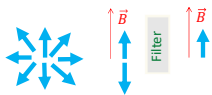
Polarization Configurations & Capabilities

Tutorial

Configuration Ingredients: Neutron Polarization Optics

Polarization Filters

- 'Quantum' has its advantages...
 - Unpolarized classical has arrows pointing everywhere
 - In ambient field, though, a quantum superposition of 'up' & 'down'
 - A filter can achieve up to *50% transmission



*Actual transmission varies widely...

Guide fields & Nutators

- Larmor precession, via torque $\vec{\tau}$ on neutron magnetic moment $\vec{\mu}$ by applied magnetic field \vec{B}

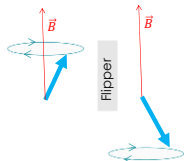
$$\vec{\tau} = \vec{\mu} \times \vec{B}, \omega = -\gamma B$$

$$\gamma = -1.833E4 \text{ rad/Gauss-sec}$$
- Frequency ω is INDEPENDENT of polar angle φ between applied field and moment
- Magnetic 'guide' fields keep $\vec{\mu}$ either aligned or anti-aligned with respect to \vec{B}
 - Keeps ω fast while changing direction of \vec{B} slowly



Flippers

- Optionally invert the neutron spin-state with respect to the ambient guide field



Strategy: Access only PARTS of the Maleev-Blume Equations

POLARIZATION CONFIGURATION	Impacts the scattered neutron	Optics
Half Polarized	Intensity	1 filter 1 flipper
Longitudinal Analysis I	Polarization State	2 filters 1 flipper
Longitudinal Analysis II Spherical Neutron Polarimetry	Both	2 filters 2 flippers

	Nuclear structure factor
$N(Q) = \sum_{R_n} b_n e^{iQ \cdot R_n}$	"IM perpendicular"
$M_{\perp} = e_Q \times M(Q) \times e_Q$	Fourier transform of magnetic moments / magnetic structure factor
$M(Q) = \sum_{R_n} M_n e^{iQ \cdot R_n}$	Unit vector along momentum transfer Q
$e_Q = Q/ Q $	Spin incoherent scattered intensity
I_{ii}	Initial and final polarization
P, P'	

$$P = 2\langle \sigma_n \rangle$$

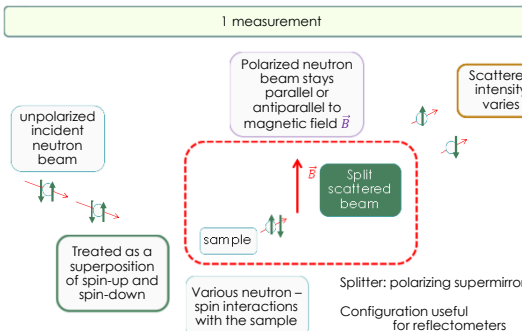
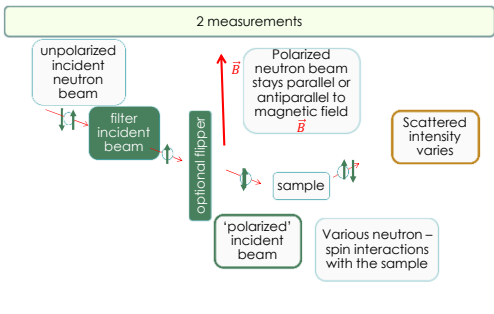
$$|P| < 1$$

- Eliminate terms based on system knowledge
- Becomes a streamlined linear algebra problem
- Capabilities: solutions to streamlined equations

$$I = I_n + N^T N + I_{ii} + M_{\perp}^T M_{\perp} + P \cdot M_{\perp}^T N + P \cdot M_{\perp} N^T + iP \cdot (M_{\perp}^T \times M_{\perp})$$

$$P'I = P \left(I_n + N^T N - \frac{1}{3} I_{ii} \right) + (P \cdot M_{\perp}^T) M_{\perp} + (P \cdot M_{\perp}) M_{\perp}^T - P(M_{\perp}^T M_{\perp}) + iN(P \times M_{\perp}^T) - iN^T(P \times M_{\perp}) + NM_{\perp}^T + N^T M_{\perp} - i(M_{\perp}^T \times M_{\perp})$$

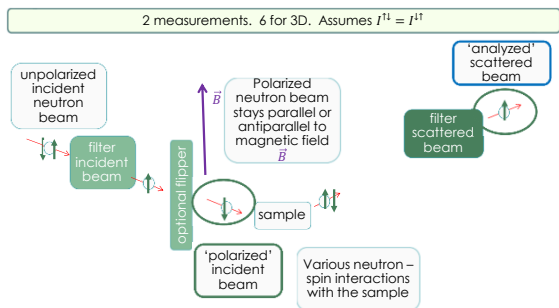
Half Polarized Configuration (intensity only; sample is always saturated in a magnetic or spin sense)



Capability table

- ★ Separate magnetic susceptibility from nuclear and spin-incoherent signal
- ★ Solve the phase problem using an additional magnetic layer
- ★ Identify coinciding of nuclear and magnetic coherent scattering in reciprocal space
- ★ Identify presence but not direction of a magnetic chiral structure
- ★ Magnon energy gain OR energy loss
- ★ Enhance coherent scattering contrast and S/N for hydrogen via Dynamic Nuclear Polarization

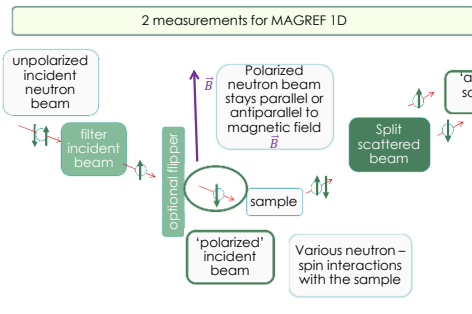
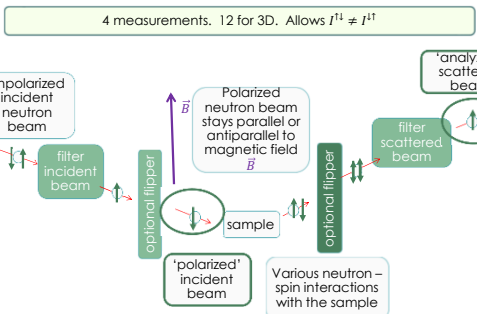
Longitudinal Polarization Analysis 1 Configuration (changes in polarization state only, spin flip & non-spin flip only)



Capability table

- ★ Separate nuclear scattering from spin-incoherent scattering
- ★ Separate spin-incoherent scattering from nuclear scattering
- ★ Determine quickly whether a signal is magnetic in origin
- ★ Track an order parameter for ferromagnetism of a powder via depolarization of thru beam
- ★ Separate nuclear scattering from both spin-incoherent scattering and magnetic scattering
- ★ Separate spin-incoherent scattering from both nuclear scattering and magnetic scattering
- ★ Quantify the isotropic magnetic moment magnitude via separation from nuclear and spin-incoherent scattering
- ★ Quantify the magnetic moment magnitude and direction and separate it from both nuclear and spin-incoherent scattering
- ★ Enhance coherent scattering contrast and S/N for hydrogen and Separate from spin-incoherent scattering

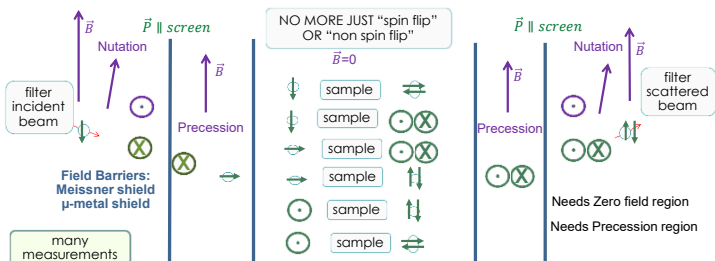
Longitudinal Polarization Analysis 2 Configuration (changes in both intensity and polarization state, spin flip & non-spin-flip only)



Capability table

- ★ Quantify magnetic moment and direction
- ★ Quantify 3D aspect of the coinciding of nuclear and magnetic coherent scattering in reciprocal space
- ★ Partly quantify chiral magnetic structure or dynamics

Spherical Polarimetry Configuration (beyond 'spin-flip' and 'non-spin-flip')



Magnetic structure factor tensor

$$\begin{pmatrix} \odot & \otimes & \odot \\ \otimes & \odot & \otimes \\ \odot & \otimes & \odot \end{pmatrix}$$

Capability table

- ★ Quantify magnetic moment and direction
- ★ Quantify 3D aspect of the coinciding of nuclear and magnetic coherent scattering in reciprocal space
- ★ Quantify magnitude and direction of chiral magnetic structure or dynamics
- ★ Insight into magnetic domains
- ★ Best approach for polarization analysis of any superconducting sample of unusual shape

Neutron Polarization Optics & Competencies

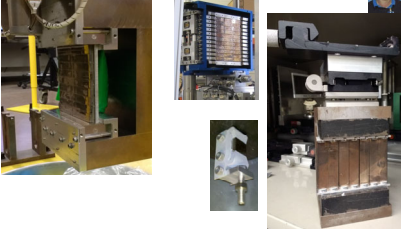
Polarization Steering Committee & Neutron Optics & Polarization Group, 2024

J. Leiner, B. Winn

FILTERS & SPLITTERS

Polarization filters select those neutrons with one of two quantum polarization states, with respect to an ambient magnetic field, via transmission, reflection or diffraction. Polarization splitters reflect neutrons of one polarization state while transmitting the other. Different filters utilize different physics, are optimal in different neutron wavelength or energy ranges, have different angular acceptances, transmission, and degrees of polarization, and may or may not be compatible with strong stray magnetic fields.

HEUSLER CRYSTALS



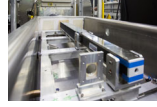
Magnetically saturated Heusler (Cu_2MnAl) crystals have a (111) Bragg peak which has nearly complete constructive (destructive) interference between nuclear and magnetic scattering lengths, depending on neutron spin state. This optic can then double as a diffraction crystal and as a polarization filter simultaneously.

At ORNL we utilize single crystals grown at ILL (a skill no longer available). ORNL provides crystal characterization and yoked assemblies, and shares several stand-alone standards for polarization characterization between instruments. Heusler arrays are used at PTAX and HYSPEC.

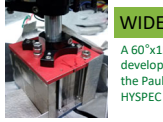
SUPERMIRROR ARRAYS

ORNL owns several arrays, some dedicated to specific instruments & others shared (available via the NOP Group). The NOP group helps instrument teams prepare specifications for mirror purchases.

SINGLE MIRROR

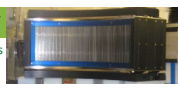


CURVED BENDERS

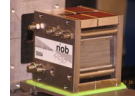


WIDE-ANGLE ARRAY

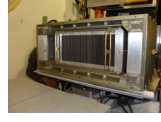
A $60^\circ \times 15^\circ$ wide angle array was developed and constructed by the Paul-Scherrer Institut for HYSPEC



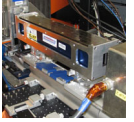
S-BENDERS



FAN ANALYZER



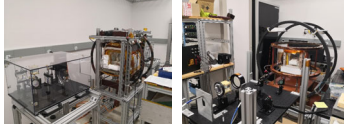
V-CHANNEL



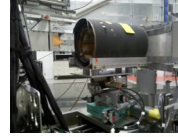
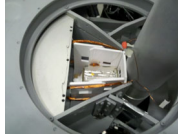
^3He FILTER

These filters co-align the nuclei of ^3He atoms. Those neutrons with spin anti-parallel to the ^3He nuclei spin are preferentially absorbed. High field uniformity and special glass surfaces are required to minimize ^3He depolarization. The NOP group provides operational support for drop-in cells, and in-situ systems, in active development for a decade, provide stable, low maintenance performance.

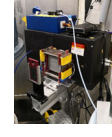
SPIN-EXCHANGE OPTICAL PUMPING (SEOP) CHARGING STATIONS



DROP IN



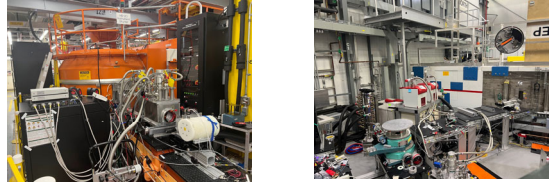
IN-SITU



LOW ABERRATION COILS



POLARIZATION DEVELOPMENT STATIONS @ HFIR



GUIDE FIELDS & NUTATORS

Guide fields provide ambient magnetic field (10-50 Gauss) in the neutron flight path, parallel or anti-parallel to the neutron moment, in which the neutron experiences Larmor precession. If the precession frequency is fast with respect to changes in the guide field direction, the neutrons 'nutate' or remain aligned with the changing guide field.

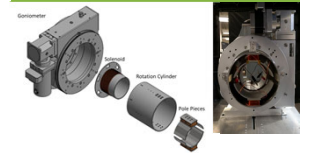
YOKED /w PM



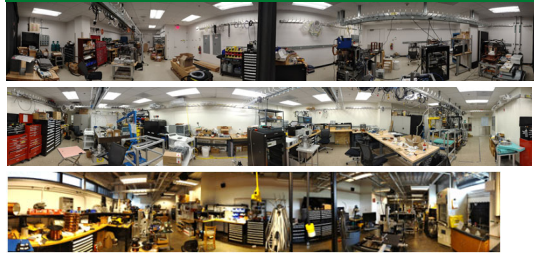
3D COILS



NUTATORS



DEVELOPMENT LABS @ SNS



FLIPPERS

Flippers change the neutron polarization with respect to the ambient guide field, between parallel and anti-parallel. Some flippers can in principle establish other neutron polarization directions but when using a guide field this depolarizes the beam.

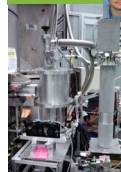
MEZEI



RF



CRYO



^3He FILTER ADIABATIC FAST PASSAGE



ZERO-FIELD CHAMBERS & PRESSION CHAMBERS

Zero-field chambers are required for the Spherical Neutron Polarimetry configuration, useful for measuring off-diagonal elements of the polarization tensor. They are also useful for studying materials in the superconducting state with polarized neutrons, since they establish a separate and well-defined Meissner screen geometry. Precession chambers utilize superconducting coils and Meissner screens to achieve conditions analogous to the 'compensation' coil of Mezei flippers, and enable neutron orientations not parallel to the precession chamber surfaces. At ORNL, we utilize a combination of μ -metal (room temperature or below), YBCO film on flat substrates (20 K with 1st stage CCR), and/or Niobium foil (<8 K with 2nd stage CCR) to achieve these conditions. The SNP system is already available via the user program for PTAX, and will be at GP-SANS once polarization filters are implemented in a planned upgrade. Wide-angle SNP is a configuration undergoing active development and design.

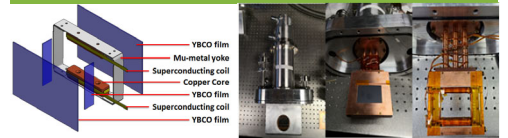
μ -METAL



CRYOSTATS



PRESSION CHAMBER /W YBCO MEISSNER SCREENS



LARMOR COMPONENTS

Larmor components enable Larmor labeling or encoding, for enhanced sensitivity to a neutrons speed or direction. In contrast to guide fields and nutators, Neutron Spin Echo (NSE) coils and Wollaston prisms establish a magnetic field perpendicular to the neutron polarization. The Mezei flipper or precession chamber concepts can be modified to create a $\pi/2$ rotation from guide field to precession field.

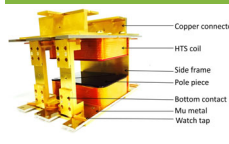
NSE COILS



CRYOSTATS



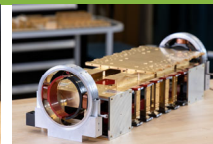
YBCO WOLLASTON PRISM



FAST DETECTORS

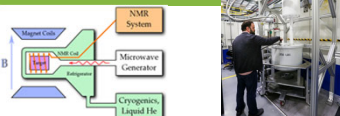


SUPERCONDUCTING RF FLIPPERS



DYNAMIC NUCLEAR POLARIZATION

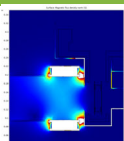
SYSTEM TO POLARIZE HYDROGEN NUCLEI



SOFTWARE

MODELING & DESIGN

The NOP Group utilizes both MAGNET[®] and COMSOL[®] for 3D magnetic modeling, and McStas¹ for polarized neutron optics design.

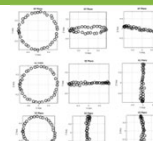


EXPERIMENT PLANNING

A variety of planning tools have been developed for various kinds of experiments.

ACQUISITION

Acquisition² leverages EPICS at the SNS and (for now) SpICE at HFIR.



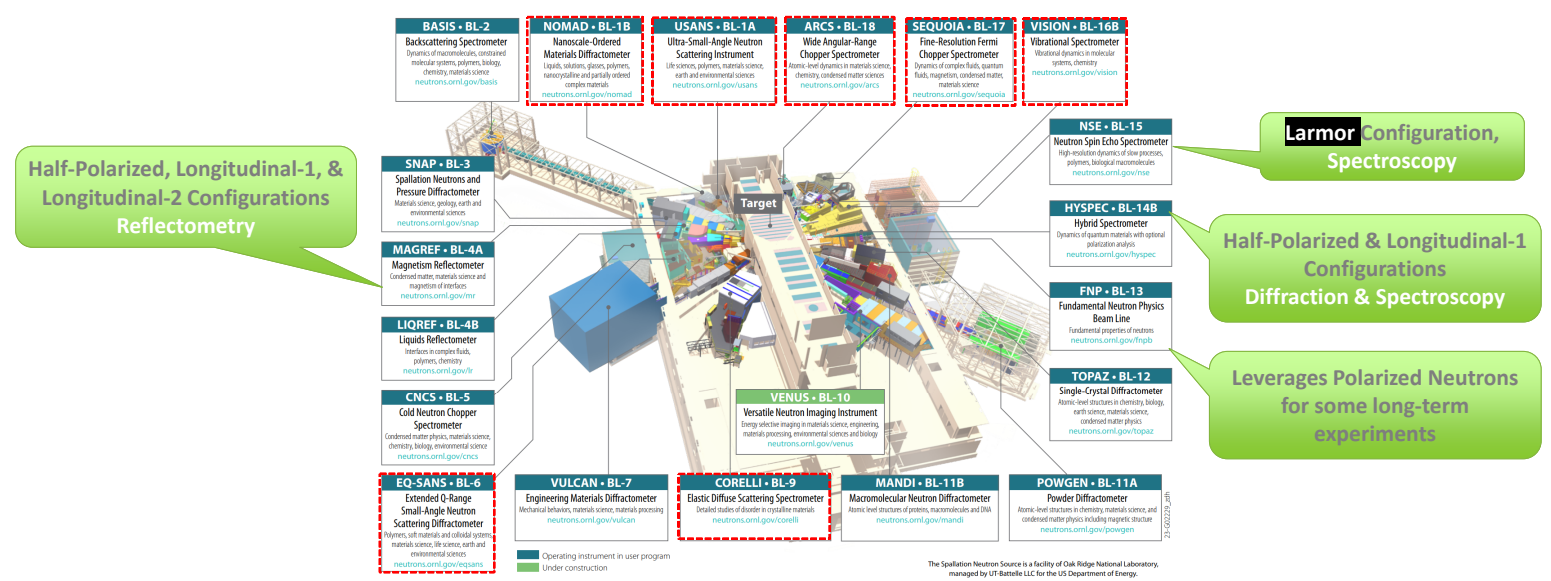
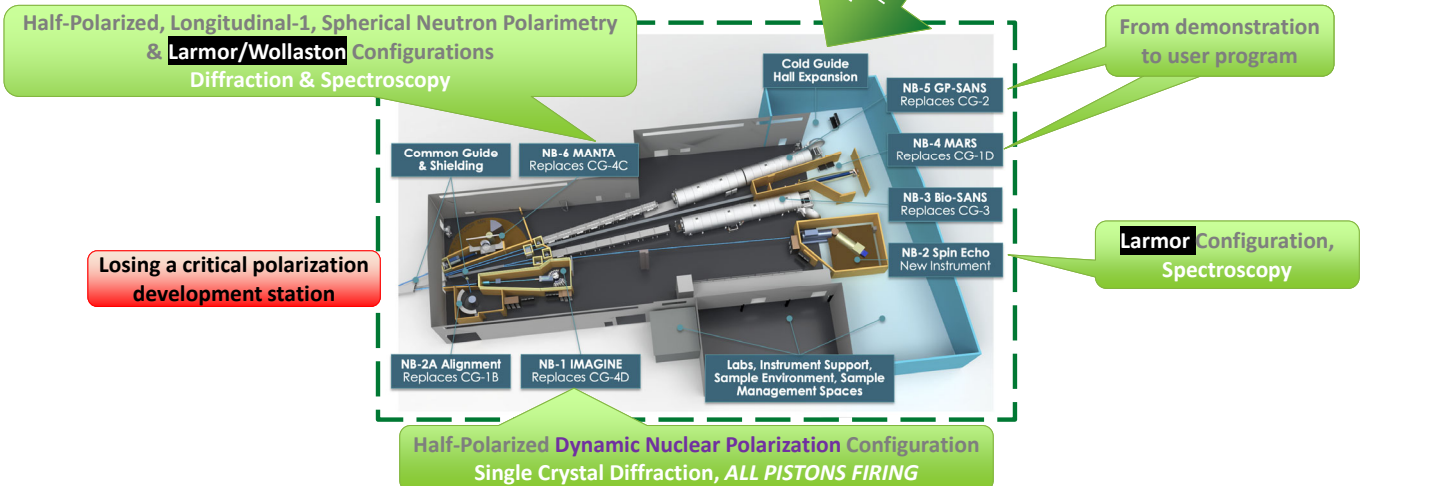
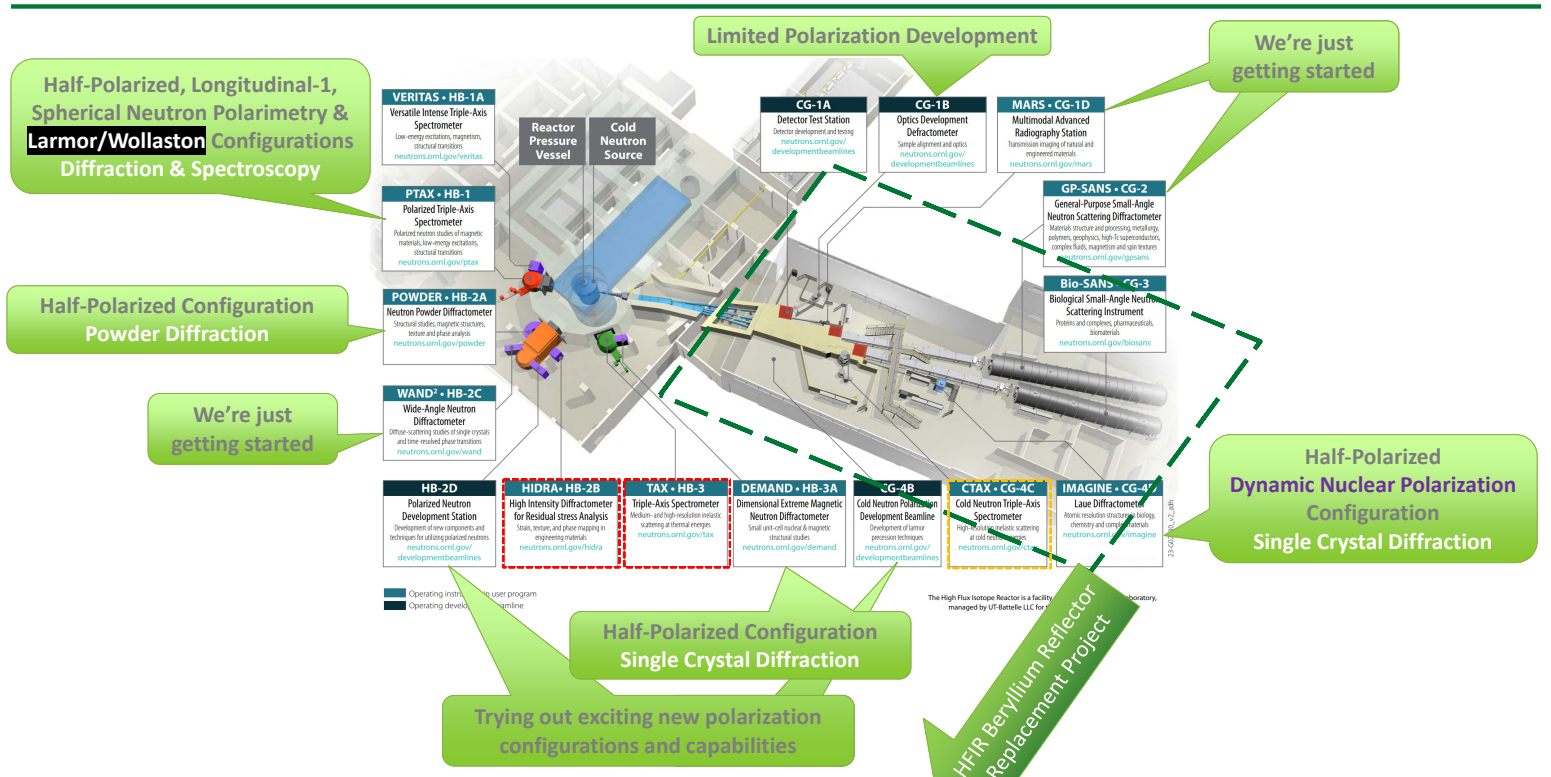
DATA REDUCTION & ANALYSIS

Reduction software has (to some extent) been integrated with the MANTID python package.

Research was performed at HFIR and SNS, DOE Office of Science User Facilities

Instruments with Polarization Configurations at HFIR & SNS

Polarization Steering Committee



Half Polarized Configuration (1 filter, 1 flipper, scattered intensity variations only) Powder & Single Crystal Diffraction

2024

The Half-Polarized Configuration is readily accessible at several instruments via the user program.
Exciting new contrast-enhancing Capabilities and Applications are on the horizon.

MALEEV-BLUME EQUATION FOR SCATTERED INTENSITY

$$I = N^{\dagger}N + I_{SI} + M_{\perp}^{\dagger}M_{\perp} + P \cdot M_{\perp}^{\dagger}N + P \cdot M_{\perp}N^{\dagger} + iP \cdot (M_{\perp}^{\dagger} \times M_{\perp})$$

With both polarized neutrons and polarized nuclei, one can shift scattered intensity from spin incoherent scattering to nuclear coherent scattering (and we're hiding a P)

Independent of polarization state so not directly used for half polarized work

Magnetization density and local site magnetic susceptibility in paramagnets, ferrimagnets and ferromagnets, and interference of magnetic and nuclear scattering

Chiral magnetic structures in antiferromagnets

$N(Q) = \sum_n b_n e^{iQ \cdot R_n}$	Nuclear structure factor
$M_{\perp} = e_Q \times M(Q) \times e_Q$	"M perpendicular"
$M(Q) = \sum_n M_n e^{iQ \cdot R_n}$	Fourier transform of magnetic moments / magnetic structure factor
$e_Q = Q/ Q $	Unit vector along momentum transfer Q
I_{SI}	Spin incoherent scattered intensity
P, P^{\dagger}	Initial and final polarization

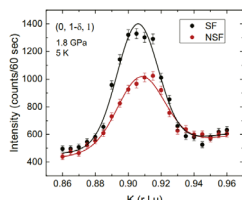
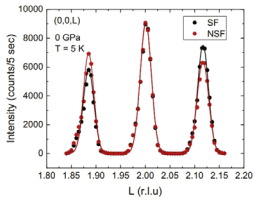
PTAX (HB-1, HFIR)



Science Area	Condensed matter
Science Example	MnP single crystal, helical magnet which exhibits superconductivity under high pressure
Capability Family	Explore magnetic chirality
Relevant M-B terms	$iP \cdot (M_{\perp}^{\dagger} \times M_{\perp})$
Capability	Chirality
Application	By aligning the neutron spin parallel and antiparallel to h, the magnetic intensities from two helical domains with clockwise and counter-clockwise helicities can be observed, respectively

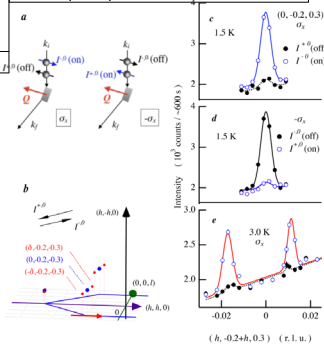
Science Area	Condensed matter
Science Example	EuPtSi single crystal, skyrmion material
Capability Family	Explore magnetic chirality
M-B	$iP \cdot (M_{\perp}^{\dagger} \times M_{\perp})$
Capability	Chirality
App. St.	Evaluate existence of chirality and its domain population

M. Matsuda et al., *Physica B* 551 115 (2018)

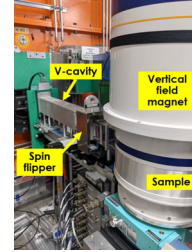


Neutron diffraction intensities in the NSF and SF channels around the (0, 0, 2 ± δ) magnetic Bragg reflections at 5 K and at ambient pressure (a) and the (0, 1 - δ, 1) magnetic Bragg reflection at 5 K and at 1.8 GPa (b)

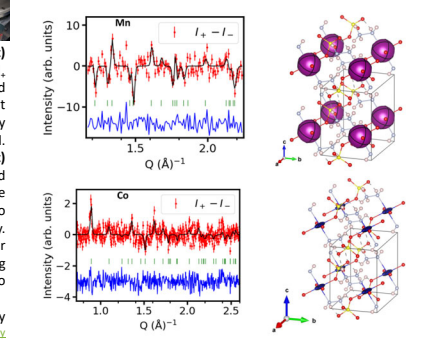
(a) Schematic drawing of the half polarized scattering setup at HB-1. Neutron spin is polarized parallel=antiparallel to the scattering vector Q. Setup for was realized by reversing the sign of the guide field. (b) Illustrative scan trajectory and positions of magnetic peaks in the ground state (blue) and the intermediate phase (red) with respect to the horizontal δ ; h; iP scattering plane. (c)-(e) Incident polarization dependence of scans along δ ; h; δ ; δ across δ ; 0; 2; 0; 3 μ measured at (c) 1.5 K, (d) 1.5 K with reversed guide field, and (e) 3.0 K with original guide field.



POWDER (HB-2A, HFIR)



Sc. A.	Condensed matter
Sc. Ex.	$M(N_2H_5)_2(SO_4)_2$ powder, metal-organic frameworks (MOF's) with 1D spin chains
Cap. Fam.	Explore magnetic scattering
M-B	$P \cdot M_{\perp}^{\dagger}N + P \cdot M_{\perp}N^{\dagger}$
Cap.	Determine local site susceptibility tensor
App. St.	Show different site anisotropy for $M=Cu^{2+}, Co^{2+},$ or Mn^{2+}



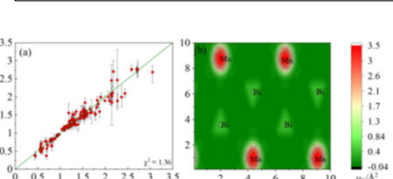
The magnetization ellipsoid representation of the local site susceptibility for the Mn & Co ion, respectively. Isotropic Heisenberg behavior for Mn and Anisotropic Ising behavior for Co

Analysis performed with CrysPy <https://sites.google.com/view/cryspy>

DEMAND (HB-3A, HFIR)



Sc. A.	Condensed matter
Sc. Ex.	$MnBi_4Te_5$ single crystal, a 2D van der Waals system and magnetic topological insulators rendering quantum anomalous Hall effect and diverse topological states
Cap. Fam.	Explore magnetic scattering
M-B	$P \cdot M_{\perp}^{\dagger}N + P \cdot M_{\perp}N^{\dagger}$
Cap.	Determine magnetization density
App. St.	Flipping ratio of 136 reflections enables conversion to magnetization density

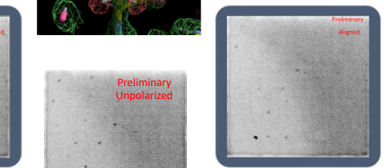
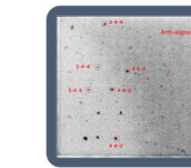
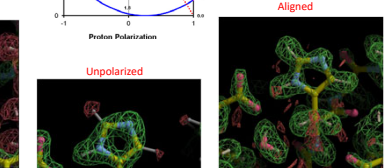
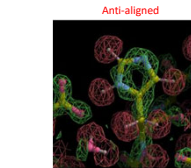
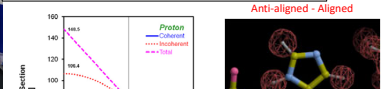


(a) The observed and calculated flipping ratios using 136 reflections. (b) Projection of the spin density within the unit cell on the (ab)-plane for $MnBi_4Te_5$, under the magnetic field of 0.83 T.

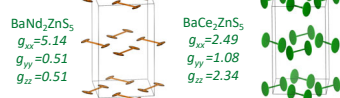
IMAGINE (CG-4D, HFIR)



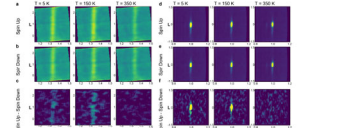
Sc. A.	Biology
Sc. Ex.	wt* T4L single crystal
Cap. Fam.	Dynamic Nuclear Polarization
M-B	$N^{\dagger}N + I_{SI}$
Cap.	Dynamic Nuclear Polarization
App. St.	J. Pierce et al, in preparation



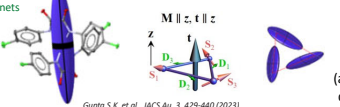
Quantum magnets



Magnetic diffuse scattering



Molecular magnets



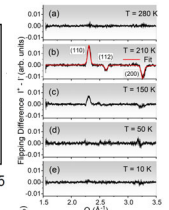
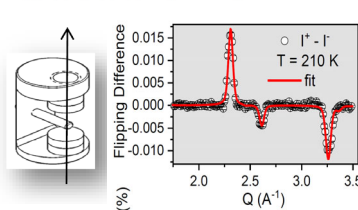
Gupta S.K. et al., *JACS* Au, 3, 429-440 (2023).

HYSPEC (BL-14B, SNS)

Sc. A.	Condensed matter
Sc. Ex.	$La_{0.4}Ce_{0.6}Co_2P_2$ powder, a weak ferromagnet which vanishes at a structural transition
Cap. Fam.	Explore magnetic scattering
M-B	$P \cdot M_{\perp}^{\dagger}N + P \cdot M_{\perp}N^{\dagger}$
Cap.	Determine Magnetization Density
App. St.	Measure weak 0.15(1) μ_B per Co atom



$$\vec{H} // \vec{P} // z \quad (\sim 0.5 T)$$



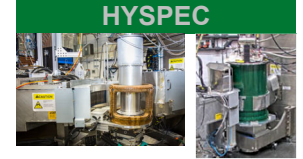
$La_{0.4}Ce_{0.6}Co_2P_2$ undergoes a weak ferromagnetic ordering at $\sim 225 K$ (~ 0.15 mB per Co atom) followed by a structural collapse at $\sim 190 K$, which leads to a strong suppression of magnetization. A combination of magnetic measurements and polarized neutron scattering experiments suggests that $La_{0.4}Ce_{0.6}Co_2P_2$ enters a disordered state with gradual dissipation of the ferromagnetic ordering taking place simultaneously with the structural collapse.



Longitudinal Polarized #1 Configuration

(2 filters, 1 flipper, spin-flip & non-spin-flip only)

Diffraction, Depolarization & Inelastic Scattering



2024

M. Matsuda, O. Garlea, B. Winn

Longitudinal-1 and 3D Polarization Analysis Configurations are readily accessible at these two spectrometers via the user program. Up to 8 T applied vertical field at both instruments is compatible with a 1D configuration, up to 0.8 T horizontal field via permanent magnet yoked systems is available, and for a wide range of temperatures a 3D configuration enables multi-dimensional access. HYSPEC's wide-angle supermirror array analyzer enables wide-angle polarization analysis. At both spectrometers, transition between polarized and unpolarized mid-experiment is routine.

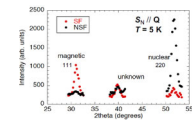
DIFFRACTION

DEPOLARIZATION

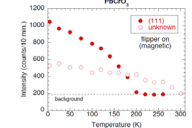
PTAX

Science Area	Condensed matter
Science Example	PbCrO ₃ powder, a perovskite with a charge-glass state
Capability Family	Isolate nuclear & magnetic scattering
Relevant M-B terms	$P N^{\dagger} N + (P \cdot M_{\perp}^{\dagger}) M_{\perp} + (P \cdot M_{\perp}) M_{\perp}^{\dagger} - P(M_{\perp}^{\dagger} M_{\perp})$
Capability	Isolate nuclear & magnetic scattering
Application Statement	Clarify nature of anomalous peak

R. Yu et al., *JACS* **137**, 12719 (2015)

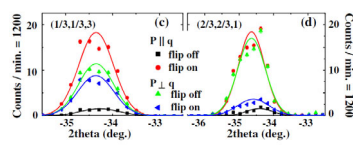


The 111 peak is magnetic in origin, but since the transition temperature is different from that of PbCrO₃, it should be attributed to the secondary phase, most probably to Pb₂CrO₅



Sc. A.	Condensed matter
Sc. Ex.	Ba ₂ CoB ₂ O ₇ single crystal, a spin-1/2 equilateral triangular-lattice antiferromagnet
Cap. Fam.	Explore magnetic scattering
M-B	$(P \cdot M_{\perp}^{\dagger}) M_{\perp} + (P \cdot M_{\perp}) M_{\perp}^{\dagger} - P(M_{\perp}^{\dagger} M_{\perp})$
Cap.	Determine spin directions
App. St.	Determine that the spins are in the ab plane

J. Ma et al., *Phys. Rev. Lett.* **116** 0872011 (2016)

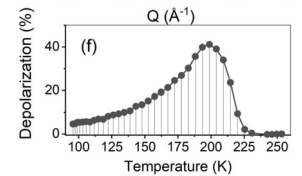
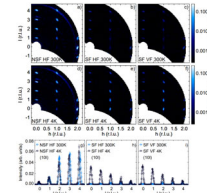


Index	I _{SF} /I _{NSF}	ab plane model	ac plane model
[2/3 2/3 1]	0.16(2)	0.12	0.88
[1/3 1/3 1]	0.36(3)	0.33	0.67
[1/3 1/3 3]	0.81(2)	0.82	0.18
[1/3 1/3 5]	0.94(2)	0.92	0.08

HYSPEC

Sc. A.	Condensed matter
Sc. Ex.	YbMnBi ₂ single crystal, a candidate Weyl metal
Cap. Fam.	Separate Mag. and Nuc. scattering
M-B	$P N^{\dagger} N + (P \cdot M_{\perp}^{\dagger}) M_{\perp} + (P \cdot M_{\perp}) M_{\perp}^{\dagger} - P(M_{\perp}^{\dagger} M_{\perp})$
Cap.	Separate magnetic and nuclear, and determine orientation of magnetic moment
App. St.	Confirm low temperature antiferromagnetic structure determined with unpolarized neutrons and refine Mn moment magnitude and direction

I. Zaliznyak et al., *J. Phys.: Conf. Ser.* **862** 012030 (2017)



The temperature dependence of the neutron depolarization factor by the sample

MALEEV-BLUME EQUATION FOR SCATTERED NEUTRON POLARIZATION STATE

$$P^{\dagger} I = P \left(I_n + N^{\dagger} N - \frac{1}{3} I_{si} \right) + (P \cdot M_{\perp}^{\dagger}) M_{\perp} + (P \cdot M_{\perp}) M_{\perp}^{\dagger} - P(M_{\perp}^{\dagger} M_{\perp}) + iN(P \times M_{\perp}^{\dagger}) - iN^{\dagger}(P \times M_{\perp}) + NM_{\perp}^{\dagger} + N^{\dagger}M_{\perp} - i(M_{\perp}^{\dagger} \times M_{\perp})$$

Isolate nuclear coherent with isotope incoherent scattering

Isolate spin-incoherent scattering

Separate contributions of different moments in the material to magnetic scattering

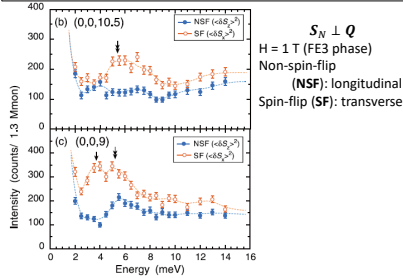
Cannot explore either nuclear magnetic interference terms or chiral structures with only spin-flip and non-spin-flip operations at the sample. These are the only options because neutron spins can only be parallel or anti-parallel to the guide field.

INELASTIC SCATTERING

PTAX with magnet

Sc. A.	Condensed matter
Sc. Ex.	Ba ₂ Mg ₂ Fe ₁₂ O ₂₂ single crystal, in field-induced noncollinear commensurate ferrimagnetic phase
Cap. Fam.	Explore magnetic scattering
M-B	$(P \cdot M_{\perp}^{\dagger}) M_{\perp} + (P \cdot M_{\perp}) M_{\perp}^{\dagger} - P(M_{\perp}^{\dagger} M_{\perp})$
Cap.	Determine orientation of magnetic excitations
App. St.	Determine that spin waves are transverse modes

T. Nakajima et al., *Phys. Rev. B* **93**, 035119 (2016)

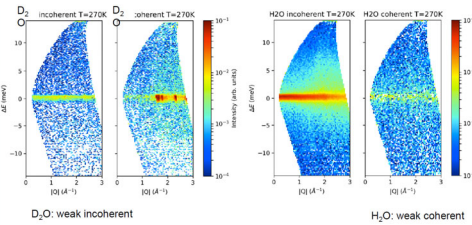


$S_N \perp Q$
H = 1 T (FE3 phase)
Non-spin-flip (NSF): longitudinal
Spin-flip (SF): transverse

HYSPEC

Sc. A.	Chemistry
Sc. Ex.	H ₂ O and D ₂ O
Cap. Fam.	Isolate spin-incoherent scattering
M-B	$P N^{\dagger} N - \frac{1}{3} P I_{si}$
Cap.	Separate nuclear scattering from spin-incoherent scattering
App. St.	Isolate autocorrelation function for both water and deuterated water

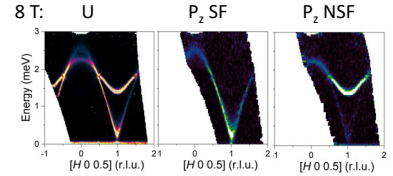
I. Zaliznyak et al, in preparation



HYSPEC with magnet

Sc. A.	Condensed matter
Sc. Ex.	Ba ₂ FeSi ₂ O ₇ single crystal, an S=1 antiferromagnet with strong easy-plane anisotropy
Cap. Fam.	Explore magnetic scattering
M-B	$(P \cdot M_{\perp}^{\dagger}) M_{\perp} + (P \cdot M_{\perp}) M_{\perp}^{\dagger} - P(M_{\perp}^{\dagger} M_{\perp})$
Cap.	Isolate transverse and longitudinal magnon modes
App. St.	Explore magnetic field dependence of longitudinal magnons near quantum critical point

S.H. Do et al, in preparation

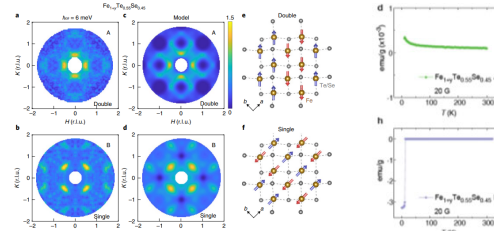


Inelastic neutron scattering on a quantum magnet at 8 Tesla magnetic field, obtained using unpolarized (left panel) and polarized neutrons (center and right panels). Polarization provides detailed information on the nature of interacting magnetic excitation modes.

HYSPEC

Sc. A.	Condensed matter
Sc. Ex.	Fe _{1-x} Te _{0.55} Se _{0.45} single crystal, ΔT~0.03
Cap. Fam.	Explore magnetic scattering
M-B	$(P \cdot M_{\perp}^{\dagger}) M_{\perp} + (P \cdot M_{\perp}) M_{\perp}^{\dagger} - P(M_{\perp}^{\dagger} M_{\perp})$
Cap.	Measure only magnetic scattering using spin-flip channel
App. St.	Measure model-matchable magnetic INS for slightly different Fe doping samples

Y. Li et al, *Nature Materials* **20** 1221 (2021)



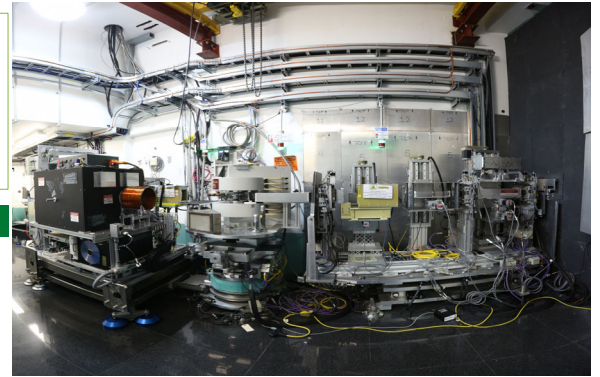
Top row A: Magnetic phase. **Bottom row B:** Superconducting phase. **a, b,** Magnetic neutron scattering (P||Q, spin-flip channel, where P is neutron spin polarization and Q is wave vector transfer) measured at 6±1 meV energy transfer where the resonance mode is observed in (b). **c, d,** Model fit using the short-range spin correlations model. **e, f,** Illustration of the Fe-Te/Se lattice and spin arrangements for the two magnetic patterns. **d, h,** Resistivity of the magnetic and superconducting phases, respectively

Polarized Neutron Reflectometry

2024

Timothy Charlton, Valeria Lauter

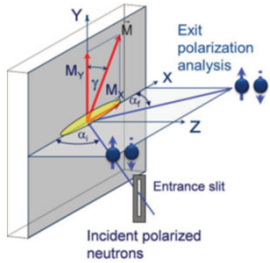
Polarized neutron reflectometry (PNR) as a unique tool that provides simultaneously high-resolution depth profile of chemical composition and of the in-plane magnetization vector and, thus, effectively probes structure and magnetization at buried interfaces and complex magnetic structures. At ORNL, the Magnetism Reflectometer (MR) is operational since 2008. MR is a time-of-flight instrument with wavelengths band of 2.5 - 12.5 Å and polarization of 98.5 - 99% of the neutron beam.



POLARIZED NEUTRON REFLECTOMETRY

- Non-destructive access to distribution of the magnetic induction along the surface normal
- Access to the lateral magnetic domain distribution
- Direct observation of anti-ferromagnetic and spiral magnetization alignments.
- Improved sensitivity in soft matter or any non-magnetic layered systems with the use of a magnetic reference layer

Reflectometry Geometry with Polarized Neutrons



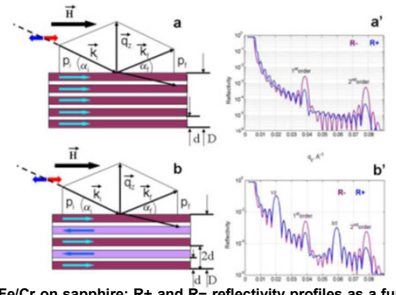
In general, $R^{\pm}(\mathbf{Q}, z)$ is the Fourier transform of the corresponding nuclear and magnetic scattering length density profiles $Nb_n(z)$ and $Nb_m(z)$ in the Z-direction, and N is the nuclear number density.

$$\left[\nabla^2 + \frac{2m_n}{\hbar^2} (E - V) \right] \psi(y) = 0$$

$$V(z) = \frac{2\pi\hbar^2}{m_n} \sum_{i=1}^{layers} N_i b_i \mp \mu_n \cdot B_i$$

$$C = m_n \mu_n / 2\pi\hbar^2 = 2.31 \times 10^{-4} \text{ nm}^{-2} \text{ T}^{-1}$$

FFT's don't work here. Must solve Schrodinger's EQ exactly.



Nanomaterials 2020, 10, 851

Courtesy of B. Toperverg

Schematic of PNR experiment with polarization analysis along the Y-axis. The ellipsoid indicates the coherence volume of neutrons defined by the beam divergence and the wavelength range.

PNR measures four reflectivities $R^{\pm}(\mathbf{Q})$ by changing the polarization direction of the incident beam and by analyzing the polarization of the reflected beam.

Non-spin-flip reflectivity:

$$R^{++} = 1/4(r^+ + r^-) + (r^+ - r^-) \cos \gamma^2$$

$$R^{+-} = 1/4(r^+ - r^-) - (r^+ - r^-) \cos \gamma^2$$

Spin-flip reflectivity:

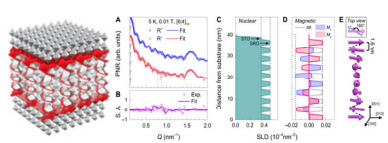
$$R^{+-} = R^{+-} = 1/4 |r^+ - r^-|^2 \sin^2 \gamma$$

a) Multilayer (ML) Fe/Cr on sapphire: R^+ and R^- reflectivity profiles as a function of momentum transfer q_z ; positions of the Bragg peaks are determined by the bilayer thickness d , the Kiessig fringes are due to the total film thickness D .
b) ML in a remanent external magnetic field resulting in the opposite alignment of the magnetization vectors in the alternating magnetic layers. b) R^+ and R^- have $1/2$ and $3/2$ -order Bragg peaks additional to ones in Fig.a, they are determined by the doubling of the magnetic part of the scattering length density profile.

Magnetism Reflectometer Examples: Half Polarized Reflectometry Configuration (1 polarizer 1 flipper)

Half Polarized Configuration (1 polarizer 1 flipper)	
Sc. A.	Condensed matter, Soft-matter with the use of a magnetic reference layer
Cap. Fam.	Explore Structure and Magnetism
Cap.	Measure small variation in the magnetic distribution under different conditions.
App. St.	Extract the structure and the in-plane magnetization vector distribution as a function of depth.

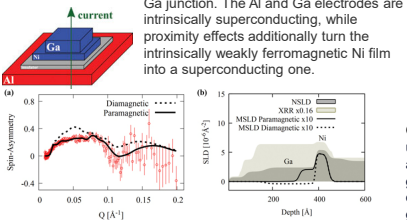
Unconventional interlayer exchange mechanism via chiral phonons in synthetic magnetic oxide heterostructures



Chiral phonons in artificial oxide superlattices mediate interlayer exchange interaction across a nonmagnetic insulator, leading to a spiral spin structure

Jeong et al., *Sci. Adv.* 8, eabm4005 (2022)
Jeong et al., *Small Methods*, accepted for publication (2023)

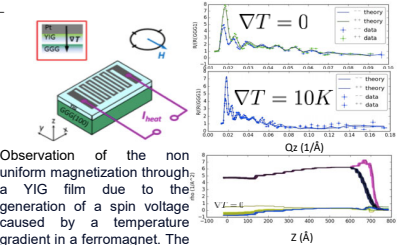
Signatures of superconducting triplet pairing in Ni-Ga-bilayer junctions



PNR results for the Ni (5.6 nm)-Ga (25 nm) bilayer delivered information about the structure and magnetization of this interface, and detected a paramagnetic Meissner response in Ga, which revealed that the proximity-coupled bilayer induces superconducting triplet pairings around the Ni-Ga interface.

Andreas Costa et al. *New J. Phys.* 24 033046 (2022)

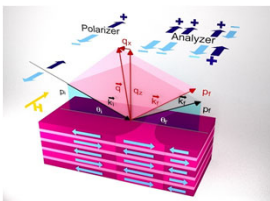
In operando PNR: Spin Seebeck effect in YIG on GGG



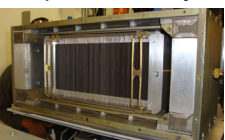
Observation of the non uniform magnetization through a YIG film due to the generation of a spin voltage caused by a temperature gradient in a ferromagnet. The temperature gradient was controlled through a resistive wire deposited on the YIG surface. The reflectivity signal was then separated by a hybrid model.

J.F.K. Cooper et al. *PRB* 96, 104404(2017)
E. Guo et al. *Phys Rev X* 6, 031012 (2016)

Magnetism Reflectometer Examples: Full Polarized Reflectometry with Off-specular Scattering Configuration (2 polarizers 2 flippers)



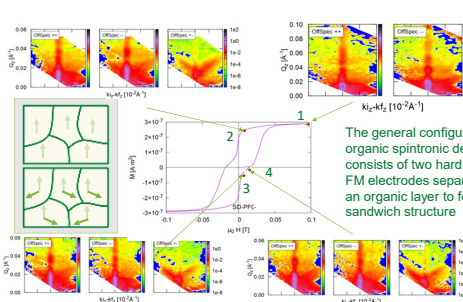
Schematic of PNR experiment with Off-Specular scattering and polarization analysis



FAN analyzer

V.G. Syromyatnikov et al. *J. Phys.: Conf. Ser.* 528 012021 (2021/4)

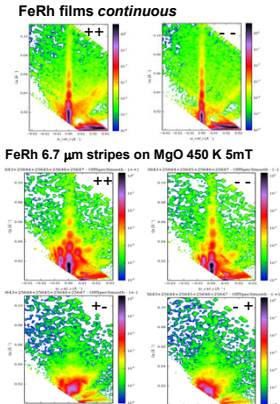
Non-collinear magnetization vector reversal in organic spin-valve SrTiO3/LaSrMnO3/(PFO)/Co/Ag



PNR and Physical Properties Measurements System (PPMS) experiments. PNR results indicated that the optimized $\text{La}_{0.7}\text{Sr}_{0.3}\text{MnO}_3$ (LSMO) and Co layers are ferromagnetic (FM) so that they can act as good soft and hard ferromagnetic electrodes in the devices.

J. Keum et al., in preparation, 2023

Magnetic Materials with tunable Properties: Magnetization configurations in continuous and patterned FeRh films



FeRh features a temperature- or field-induced metamagnetic transition from the antiferromagnetic order (AF) to the ferromagnetic order (FM) that occurs at 370 K at zero magnetic field. Strong spatial confinement and strain have a significant impact on the phase coexistence and reversal dynamics of the transition.

PNR established that a residual positive moment in thin films in the AF phase originates from interfaces, most likely a result of strain and disorder. The reflectivity fitting of stripes suggest behavior similar to a continuous film, but with addition of defects throughout the depth of the film, likely at the wire edges, which influence the FeRh phase and transition.

Sheena Patel et al., in preparation, 2023

Polarized Neutrons & X-Ray Dichroism: Complementary Diagnostics for Magnetism

2024

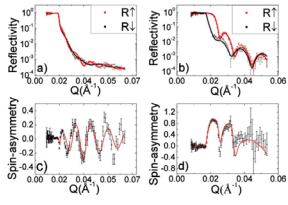


FIG. 3. (Color online) Polarized neutron reflectivity recorded with an applied field of $\mu_0 H = 0.34$ T at (a) 300 K and (b) 400 K. (c) and (d) are the spin asymmetry at 300 K and 400 K, respectively.

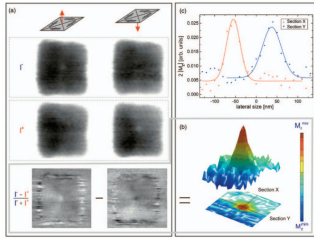


FIG. 2. (Color Panel) (a) shows the static configuration of a vortex structure (sample A: 500 × 500 nm², 40 nm thick) with a vortex core pointing up (left column) and down (right column). In the first row, images were taken for negative polarization of the photons (I^-) while images with opposite polarization (I^+) are shown in the second row. The "dichroic image" is depicted in the third row. A white or black spot can be observed, corresponding to a vortex core pointing up or down, respectively. The two dichroic images were subtracted from one another and a 3D image is given in panel (b) (200 × 200 nm² cut). The distributions along sections X and Y are plotted in panel (c) with the corresponding Gaussian fits in order to estimate the size of the vortex core.

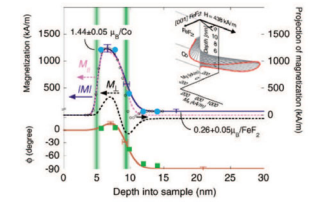


Figure 4. Depth dependence of the vector magnetization (inset, 3D view), magnitude (blue curve, $|M|$), and angular deviation ϕ (red curve) from the applied field in the sample plane deduced from neutron scattering. Error bars represent deviations of depth profiles with indistinguishable χ^2 . The magnetization used in the OOMMF simulation is indicated by \bullet and the values of ϕ are indicated by \blacksquare obtained from the simulation. The sum of the Fe and Co spin density profiles of $I(100) \parallel \text{FeF}_2$ (obtained from figure 2 in arbitrary units using X-ray scattering) is shown in absolute units (e).

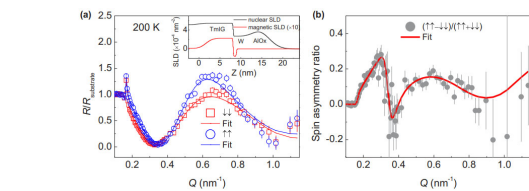


FIG. 4. Capturing the spin textures in the W5 (nm)/TmG (10 nm) by neutron techniques at 200 K. (a) Polarized neutron reflectivities (with a 700-mT in-plane field) for the spin-polarized $R^{\uparrow\uparrow}$ and $R^{\uparrow\downarrow}$ channels. Inset: Corresponding models with structural and magnetic scattering length densities (SLDs) used to obtain the best fits. (b) The spin asymmetry ratio ($R^{\uparrow\uparrow} - R^{\uparrow\downarrow} / (R^{\uparrow\uparrow} + R^{\uparrow\downarrow})$) between the $R^{\uparrow\uparrow}$ and $R^{\uparrow\downarrow}$ channels. The error bars are ± 1 s.d.

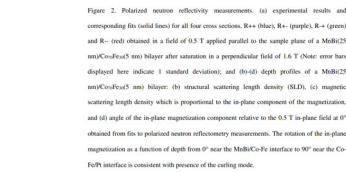
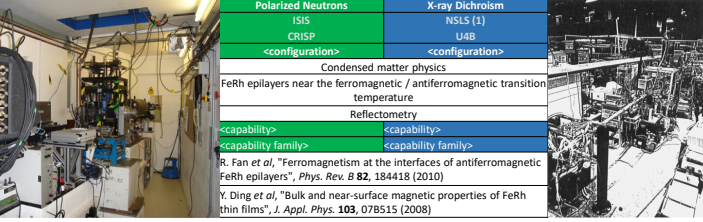


Figure 2. Polarized neutron reflectivity measurements. (a) experimental results and corresponding fits (solid lines) for four cross-sections, R_{ex} (black), R_{y} (purple), R_{z} (green) and R_{z} (red) obtained in a field of 0.5 T applied parallel to the sample plane of a MnBi2Sb (50 nm)/CuNiFe (5 nm) bilayer after saturation in a perpendicular field of 1.6 T (Note: error bars displayed here indicate 1 standard deviation); (b)-(d) depth profiles of a MnBi2Sb (50 nm)/CuNiFe (5 nm) bilayer: (b) structural scattering length density (SLD), (c) magnetic scattering length density which is proportional to the in-plane component of the magnetization, and (d) angle of the in-plane magnetization component relative to the 0.5 T in-plane field at θ^* obtained from fits to polarized neutron reflectivity measurements. The rotation of the in-plane magnetization as a function of depth from 0° near the MnBi2Sb/CuNiFe interface to 90° near the CuNiFe interface is consistent with presence of the capping mode.



Polarized Neutrons	X-ray Dichroism
ISIS	NLSLS (1)
CRISP	U4B
<configuration>	<configuration>
Condensed matter physics	
FeRh epilayers near the ferromagnetic / antiferromagnetic transition temperature	
Reflectometry	
<capability>	<capability>
<capability family>	<capability family>
R. Fan et al., "Ferromagnetism at the interfaces of antiferromagnetic FeRh epilayers", <i>Phys. Rev. B</i> 82 , 184418 (2010)	
Y. Ding et al., "Bulk and near-surface magnetic properties of FeRh thin films", <i>J. Appl. Phys.</i> 103 , 07B515 (2008)	

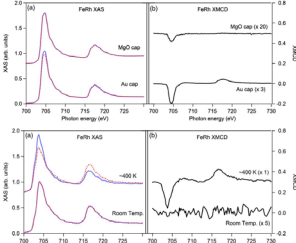


FIG. 3. (Color online) Ambient and elevated temperature XAS spectra of a 500 Å FeRh film on MgO (001) coated with 20 Å of Au. (a) XAS spectra for FeRh at 200 K. (b) XAS spectra for FeRh at 300 K. Note the scale factors.

Polarized Neutrons	X-ray Dichroism
Lujan Neutron Scattering Center	Advanced Light Source
Asterix spectrometer in GI-SANS mode	Scanning Transmission X-ray Microscope (STXM) beamline
Half Polarized and Longitudinal 1	X-ray circular dichroism
Condensed matter	
Fe dots with transition from single domain to vortex as a function of dot diameter and magnetic field	
$\text{Ni}_{50}\text{Fe}_{50}$ permalloy thin film (40 nm) with single magnetic vortex	
Small Angle Neutron Scattering	Soft X-ray Microscopy
Depth profile	Transverse profile
IV. Roshchin et al., "Measurement of the vortex core in sub-100nm Fe dots using polarized neutron scattering", <i>EPL</i> 86 67008 (2009)	
K.W. Chou et al., "Direct Observation of the vortex core magnetization and its dynamics", <i>App. Phys. Lett.</i> 90 , 25205 (2007)	

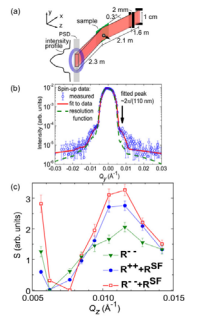


Figure 3. Spin density depth profiles for Co (blue) and Fe (red) spins obtained from the specular X-ray reflectivities at $H_{\text{ext}} = \pm 796$ kA/m.

Polarized Neutrons	X-ray Dichroism
NIST Center for Neutron Scattering	Advanced Photon Source
NGI reflectometer	4ID-D
Longitudinal 2	Circular Dichroism
Condensed matter	
Fe & Gd multilayer	
Reflectometry	
E. Kravtsov et al., "Complementary polarized neutron and resonant x-ray magnetic reflectometry measurements in Fe/Gd heterostructures: Case of inhomogeneous interlayer magnetic structure", <i>Phys. Rev. B</i> 79 134438 (2009)	

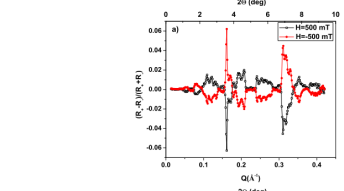


Figure 3. (Color online) (a) Resonant x-ray magnetic reflectivity spectra (asymmetry ratio) measured at the Gd_{L_2} edge ($E = 7929$ eV) at $T = 20$ K in magnetic fields 500 and -500 mT. The signals measured at opposite fields are symmetrical, which indicates their magnetic origin. (b) Experimental (circles) and fitted (line) RSMR spectra for $T = 20$ K, $H = 500$ mT. (c) Experimental (circles) and fitted (line) non-spin-flip PBR spectra for $T = 20$ K, $H = 500$ mT.

Polarized Neutrons	X-ray Dichroism
Lujan Neutron Scattering Center	Advanced Light Source
Reflectometer	Reflectometer
Longitudinal 2	circular dichroism
Condensed matter	
single crystal of antiferromagnetic FeF_2 capped with a ferromagnetic Co film	
Specular reflectivity & off-specular scattering	
spatial distribution of different vector components of the magnetization	
magnetization with element-selectivity	
S.K. Sinha et al., "Combined neutron and synchrotron studies of magnetic films", <i>Pramana-J. Phys.</i> 67 47-55 (2006)	

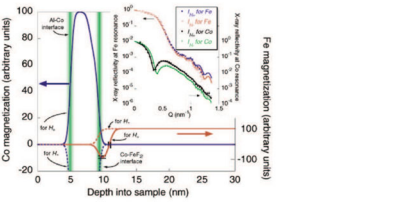
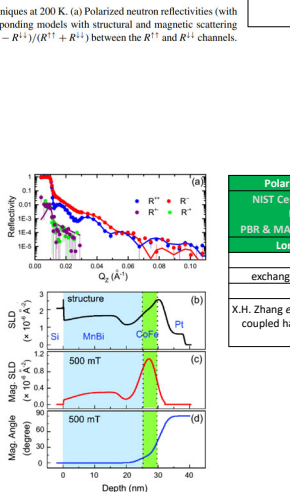
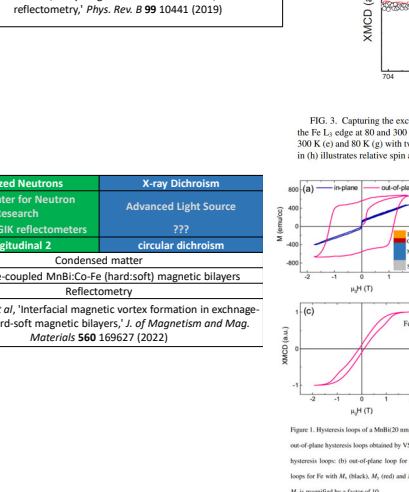


Figure 3. Spin density depth profiles for Co (blue) and Fe (red) spins obtained from the specular X-ray reflectivities at $H_{\text{ext}} = \pm 796$ kA/m.

Polarized Neutrons	X-ray Dichroism
NIST Center for Neutron Research	Advanced Light source
PBR	???
Longitudinal 2	Circular Dichroism
Condensed matter physics	
Multilayer with ferrimagnetic insulator and heavy metal layers which exhibits an anomalous Hall effect	
reflectometry	
Q. Shao et al., "Exploring interfacial exchange coupling and sublattice effect in heavy metal/ferrimagnetic insulator heterostructures using Hall measurements, x-ray magnetic circular dichroism, and neutron reflectometry", <i>Phys. Rev. B</i> 99 10441 (2019)	



Polarized Neutrons	X-ray Dichroism
NIST Center for Neutron Research	Advanced Light source
PBR	???
Longitudinal 2	Circular Dichroism
Condensed matter physics	
Multilayer with ferrimagnetic insulator and heavy metal layers which exhibits an anomalous Hall effect	
reflectometry	
Q. Shao et al., "Exploring interfacial exchange coupling and sublattice effect in heavy metal/ferrimagnetic insulator heterostructures using Hall measurements, x-ray magnetic circular dichroism, and neutron reflectometry", <i>Phys. Rev. B</i> 99 10441 (2019)	



Polarized Neutrons	X-ray Dichroism
NIST Center for Neutron Research	Advanced Light source
PBR	???
Longitudinal 2	Circular Dichroism
Condensed matter physics	
Multilayer with ferrimagnetic insulator and heavy metal layers which exhibits an anomalous Hall effect	
reflectometry	
Q. Shao et al., "Exploring interfacial exchange coupling and sublattice effect in heavy metal/ferrimagnetic insulator heterostructures using Hall measurements, x-ray magnetic circular dichroism, and neutron reflectometry", <i>Phys. Rev. B</i> 99 10441 (2019)	

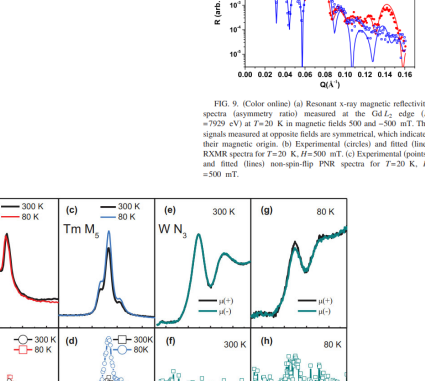


FIG. 3. Capturing the exchange interactions in the W5 (nm)/TmG (10 nm) by x-ray techniques. (a) XAS and (b) XMCD spectra taken at the Fe_{L_3} edge at 80 and 300 K. (c) XAS and (d) XMCD spectra taken on the Tm M_2 edge at 80 and 300 K. XAS taken on the W_{N_2} edge at 300 K (e) and 80 K (g) with two opposite x-ray helicities, μ^+ and μ^- . XMCD at the W_{N_2} edge taken at 300 K (f) and 80 K (h). The inset in (b) illustrates relative spin alignments of the Fe, Tm, and induced W moment at 80 K based on the sign of XMCD.

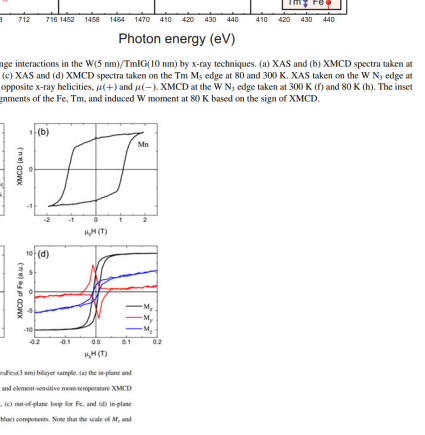


Figure 3. Hysteresis loops of a MnBi2Sb(50 nm)/CuNiFe(5 nm) bilayer sample. (a) In-plane and out-of-plane hysteresis loops obtained by VSM and element-selective room-temperature XMCD hysteresis loops. (b) In-plane loop for Mn. (c) Out-of-plane loop for Fe. (d) In-plane loops for Fe with M_x (black), M_y (red) and M_z (blue) components. Note that the scale of M_x and M_z is magnified by a factor of 10.

Development of Spherical Neutron Polarimetry for HFIR and Beyond

Chenyang Jiang¹, Nicolas Silva¹, Jacob Tosado¹, Tianhao Wang¹, Masaaki Matsuda², Barry Winn², Lowell Crow¹

¹Neutron Technologies Division, Oak Ridge National Laboratory

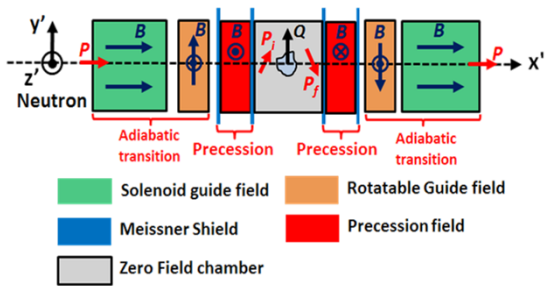
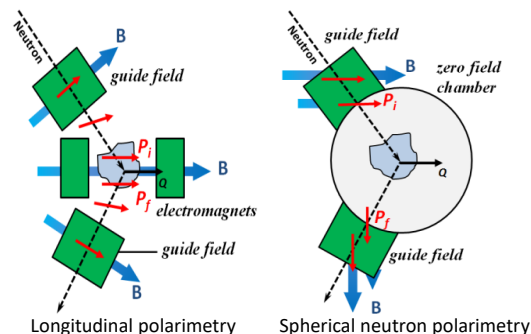
²Neutron Scattering Division, Oak Ridge National Laboratory

Motivation

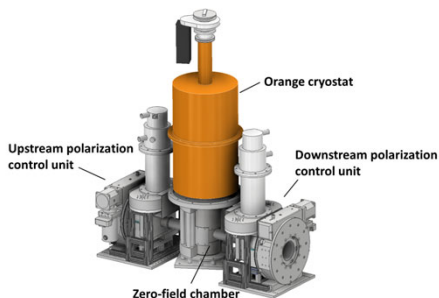
- Distinguish between polarization rotation and depolarization
- Study complex magnetic materials
 - Spin-topological matter
 - Magneto-electric crystals
 - Superconductors, etc.

Principle

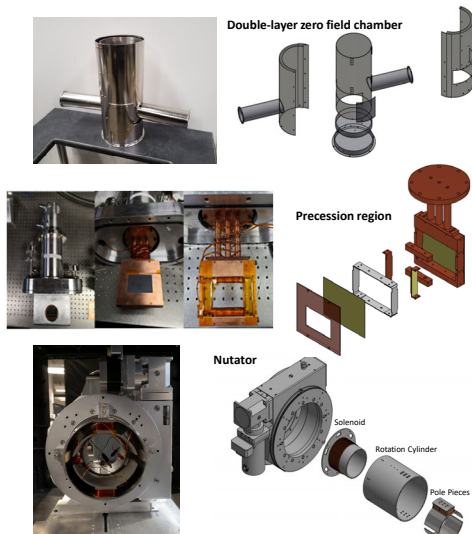
- Decouple the incoming and outgoing neutron polarization
 - Zero-field chamber
 - Combination of adiabatic and non-adiabatic transitions to control neutron polarization



Portable High-Tc Polarization Analysis Device (PHitPAD)



Essential components

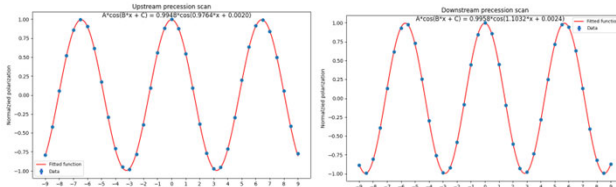
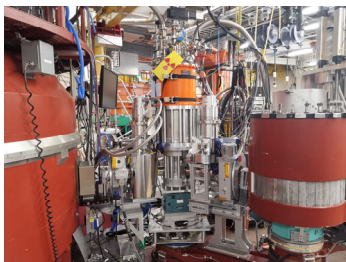


Intrinsic spin transport of the device for 13.5 meV neutrons



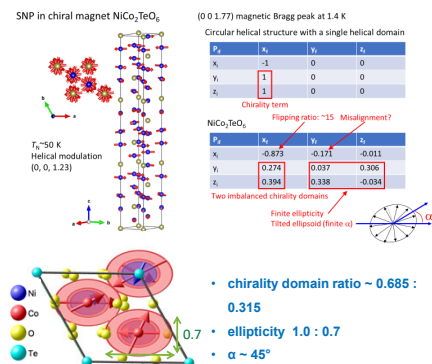
Optimize nutator current
Solve Bloch equation to calculate the spin propagation
Rotation of the angle $\sim 2^\circ$

Setup and Test at HFIR HB-1



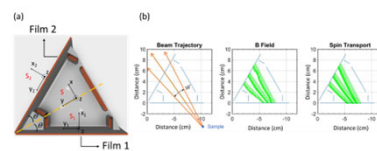
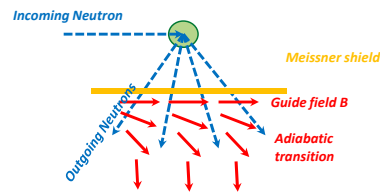
Sample	Normalized polarization matrix			Theoretical polarization matrix			
	P_x	P_y	P_z	x	y	z	
Silicon (1 1 1)	x	0.999(3)	0.039(4)	-0.025(4)	1	0	0
	y	0.022(4)	0.999(3)	-0.014(4)	0	1	0
	z	0.054(4)	0.025(4)	0.966(3)	0	0	1
BiFeO ₃ (0.5 0.5 0.5)	x	-0.939(7)	-0.017(12)	0.006(13)	-1	0	0
	y	0.029(12)	0.036(12)	0.025(13)	0	0	0
	z	0.026(12)	0.042(12)	-0.014(12)	0	0	0
Ca ₂ Y ₂ Cu ₂ O ₁₀ (0 0 1)	x	-1.005(6)	-0.003(7)	-0.007(7)	-1	0	0
	y	0.020(7)	0.995(6)	0.032(7)	0	1	0
	z	0.002(7)	-0.024(7)	-0.962(6)	0	0	-1

SNP on a Chiral magnet sample



Towards time-of-flight instruments

- No SNP device for time-of-flight instruments to date
- Neutron polarization precession is energy dependent
 - Extremely difficult to align different wavelength neutron polarization
- HYSPEC at SNS
 - Direct geometry spectrometer
 - Monochromatic incident beam
 - Polychromatic scattered beam
- SNP on HYSPEC
 - Only need to focus on the scattered beam side
 - Rely on adiabatic transition to align the neutron polarization to the analyzer



(a) The two superconducting films are forming a 60° angle to increase the angle coverage for the scattered beam, corresponding to $\theta = 30^\circ$
(b) The range of neutron trajectories with satisfactory adiabatic conditions are shown when the three sets of coils are turned on. The corresponding magnetic fields and calculated spin transports for 15 meV neutrons are also presented.

Summary

- PHitPAD in HFIR user program
- User experiments scheduled on HB-1
- Design of SNP on HYSPEC is underway

Acknowledgements: Research was performed at HFIR and SNS, two DOE Office of Science User Facilities. Parts of the research were supported by ORNL's Laboratory Directed Research and Development (LDRD) program. C.J. acknowledges the support of U.S. DOE BES Early Career Award No. KC0402010, under Contract DE-AC05-00OR22725.

Polarized Neutron applications for Biology, Soft Matter, & Chemistry

2024

Longitudinal 1 at MACS (NCNR)

Science Area	Chemistry
Science Example	Partially deuterated Methanol
Capability Family	Separate coherent and spin-incoherent scattering
Relevant terms	$PN^{\dagger}N - \frac{1}{3}PI_{st}$
Capability	Separate dynamic structure factors in a wide Q range
Application Statement	Sensitive measurement of weak coherent scattering

W. Chen *et al.*, "Wide-angle polarization analysis on the multi-axis crystal spectrometer for the study of collective and single particle dynamics of methanol at its prepeak," *Physica B: Condensed Matter* **564** 166 (2019)

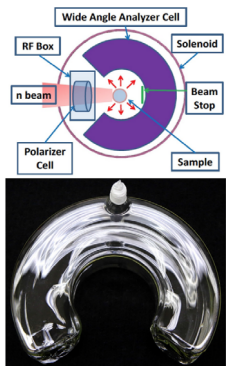


Fig. 1. Top view of the layout of the spin filter apparatus in the MACS sample area (top picture). Cold incident neutrons are polarized by a polarized ³He cell that is located in an RF end-compensated solenoid surrounded by an aluminum shielding box and focused at the sample position. After scattering from the sample, neutrons are spin-analyzed by a horn-shaped wide angle ³He analyzer (bottom picture) and detected with a 2D-detector bank system.

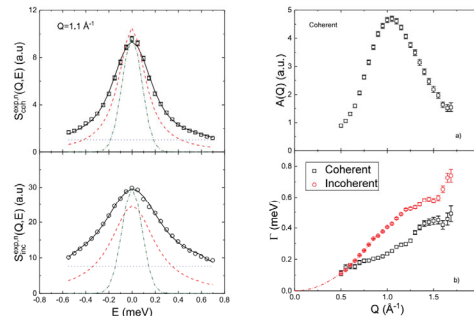


Fig. 3. (a) Fit of the experimental data according to Eq. (11) at $Q = 1.1 \text{ \AA}^{-1}$. The symbols are experimental data, the continuous black line is the fit, the red dashed, blue dotted, and green dash-dotted lines represent the Lorentzian function before convolution, the linear background, and the bright resolved resolution function respectively. (For interpretation of the references to colour in this figure legend, the reader is referred to the web version of this article.) (b) The area of the coherent spectra. Notice the location of the maximum in correspondence of the prepeak. (c) The FWHM values obtained from the fitting of the coherent and incoherent spectra using Eq. (11). The dashed red line represents the fit of the incoherent spectra width to a Fickian diffusion model in the range up to $Q = 0.65 \text{ \AA}^{-1}$. Notice how the results of the diffusion signal do not follow the Q^2 behavior of the Fickian diffusion and a slowing down of the dynamics can be observed in correspondence of the prepeak. (For interpretation of the references to colour in this figure legend, the reader is referred to the web version of this article.)

Longitudinal 1 at D7 (ILL)

Science Area	Chemistry
Science Example	Heavy Water
Capability Family	Separate coherent and spin-incoherent scattering
Relevant terms	$PN^{\dagger}N - \frac{1}{3}PI_{st}$
Capability	Separate dynamic structure factors in a wide Q range
Application Statement	Observe collective fluctuations at mesoscales

A. Arbe *et al.*, "Coherent structural relaxation of water from meso- to intermolecular scales measured using neutron spectroscopy with polarization analysis," *Physical Review Research* **2** 022015(R) (2020)

Science Area	Chemistry
Science Example	Protic Ionic Liquids
Capability Family	Separate spin-incoherent from coherent scattering
Relevant terms	$PN^{\dagger}N - \frac{1}{3}PI_{st}$
Application Statement	Compare coherent scattering to simulation for both structure and QENS

T. Burankova *et al.*, "Linking Structure to Dynamics in Protic Ionic Liquids: A Neutron Scattering Study of Correlated and Single-Particle Motions," *Scientific Reports* **8**, 16400 (2018)

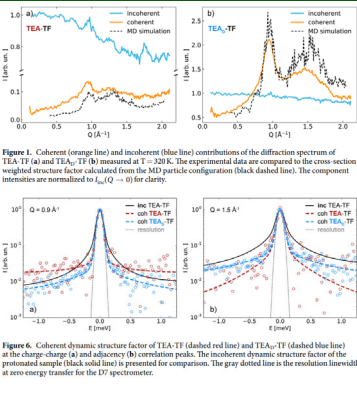


Figure 4. Coherent (orange line) and incoherent (blue line) contributions of the diffraction spectrum of TEA-TF (a) and TEA₂TF (b) measured at $T = 200 \text{ K}$. The experimental data are compared to the cross-section weighted structure factor calculated from the MD particle configuration (black dashed line). The component intensities are normalized to $I_{coh}(Q \rightarrow 0)$ for clarity. Figure 5. Coherent dynamic structure factor of TEA-TF (dashed red line) and TEA₂TF (dashed blue line) at the charge charge (a) and TEA₂TF (b) correlation peaks. The incoherent dynamic structure factor of the protic sample (black solid line) is presented for comparison. The gray dotted line is the resolution linewidth at zero energy transfer for the D7 spectrometer.

Longitudinal 1 at SANS instrument TAIKAN (BL15, J-PARC)

Science Area	Chemistry
Science Example	Colloidal particles of either TBP/(HNO ₃) ₃ or PtCl ₆ (BEHU) ₃ H ₂
Capability Family	Separate coherent and spin-incoherent scattering
Relevant terms	$PN^{\dagger}N - \frac{1}{3}PI_{st}$
Capability	Separate structure factors at low Q
Application Statement	Sensitive measurement of weak coherent scattering

T. Okudaira *et al.*, "Polarization analysis for small-angle neutron scattering with a ³He spin filter for a pulsed neutron source," *J. Appl. Cryst.* **54** 548 (2021)

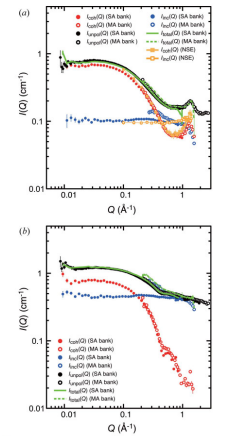


Figure 6. Double logarithmic plots of the SANS profiles obtained for the colloidal particle dispersions of (a) TBP(HNO₃) and (b) PtCl₆(BEHU)₃ complexes (samples 1 and 2). The NPA results, i.e. $I_{coh}(Q)$ (red closed and open circles) and $I_{inc}(Q)$ (blue closed and open circles) are plotted together with their sum, $I_{tot}(Q)$ (green solid and dashed lines). SANS profiles obtained using an unpolarized incident neutron beam are indicated by black closed and open circles. The NPA results obtained using an NSE spectrometer for sample 1 only are indicated in (a) by orange closed and open squares for $I_{coh}(Q)$ and $I_{inc}(Q)$, respectively, with an intensity scale factor of approximately 0.9. The abbreviations SA and MA denote the small-angle and middle-angle detector banks, respectively.

DNP / Half at IMAGINE (CG-4D, HFIR)

Sc. A.	Biology
Sc. Ex.	wt* ⁴ T4L single crystal
Cap. Fam.	Dynamic Nuclear Polarization
M-B	$N^{\dagger}N + I_{st}$
Cap.	Dynamic Nuclear Polarization
App. St.	J. Pierce <i>et al.</i> , in preparation

DNP / Half at iMATERIA (BL-20, J-PARC)

Science Area	Biology
Science Example	Hair with water, follicles aligned vertically
Capability Family	Dynamic Nuclear Polarization (with fast sample exchange)
Relevant terms	$N^{\dagger}N + I_{st}$
Capability	Vary Hydrogen polarization to explore coherent scattering of Hydrogen with different soaking conditions
Application Statement	Determine water distribution in hair

Y. Noda *et al.*, "Water distribution in human hair microstructure elucidated by spin contrast variation small-angle neutron scattering," *J. Appl. Cryst* **56** (2023)

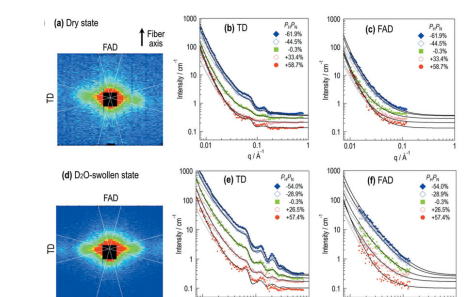
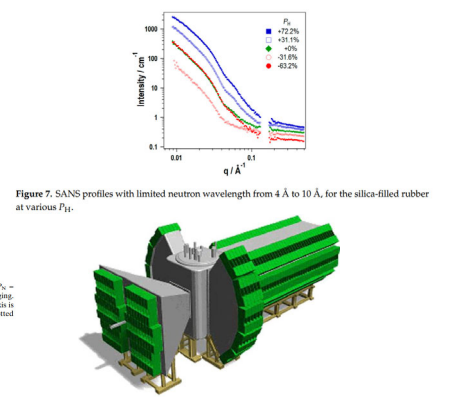


Figure 7. SANS profiles with limited neutron wavelength from 4 Å to 10 Å, for the silica-filled rubber at various P_{12} .

Science Area	Soft Matter
Science Example	Silica-filled Rubber (2 component system)
Capability Family	Dynamic Nuclear Polarization (with fast sample exchange)
Relevant terms	$N^{\dagger}N + I_{st}$
Capability	Vary Hydrogen polarization to explore coherent scattering of Hydrogen in industrial samples
Application Statement	Sample is a new standard utilized to calibrate the DNP system

Y. Noda *et al.*, "First Experiment of Spin Contrast Variation Small-Angle Neutron Scattering on the iMATERIA Instrument at J-PARC," *Quantum Beam Sci* **2020**, 33 (2020)



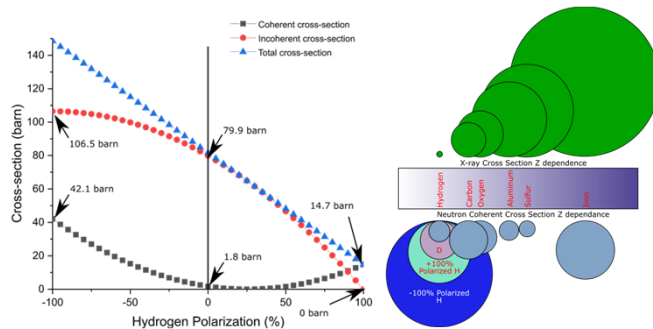
Accelerating Discovery Using DNP-Enhanced Neutron Protein Crystallography

Neutron Scattering Division: Josh Pierce, Malcolm Cochran, Flora Meilleur, Andrey Kovalevsky, Zach Morgan, Bryan Chakoumakos, Dean Myles

Neutron Technologies Division: Dominic Giuliano, Matt Loyd, Lowell Crow, Matt Frost, Amy Jones

Spin Dependence of Neutron Scattering from Hydrogen

- The spin dependence of the hydrogen cross section is large
 - For hydrogen $b = -3.74 + 14.56 \times P_n \times P_H$
- Nuclear incoherent scattering can be removed entirely (true for any nucleus)
- Coherent scattering can be increased by a factor of 7 (or 20)
- An increase in signal to noise enters **squared** in figure of merit
 - Factor of 10 in signal to noise is a factor of 100 in flux/sample size/data collection time
- The hydrogen nucleus is polarizable via Dynamic Nuclear Polarization, DNP



Breakthrough High Impact Biological Science

DNP-enhanced macromolecular crystallography will deliver >10-100 fold gains in performance for neutron analysis of hydrogenous materials, enabling breakthroughs in our understanding and control of complex biological systems

- Large >> 10-100 fold increases in S/N of the data
- Amplifying diffraction intensity and minimizing incoherent scattering background
 - Higher resolution data from radically smaller protein crystals (< 0.01 mm³)
 - More rapid data collection (hours or days)
 - Enables the visibility of hydrogen atoms to be amplified and enhanced in situ
 - New ways to collect, analyze and amplify diffraction from biological systems
- General – ALL hydrogenated proteins from ANY biological system.

Enabled Science and Capability

- Radically smaller crystals (<< 0.01 mm³)
- Larger proteins/complexes
- Membrane proteins

DNP: Amplifying/tuning Hydrogen

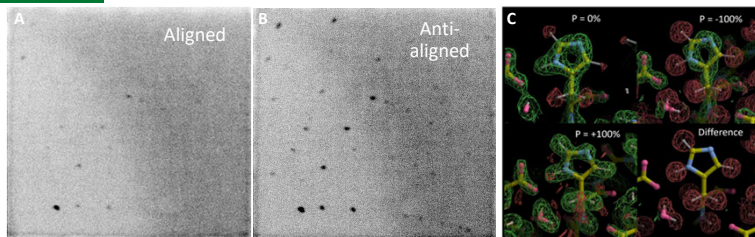
Maximizes signal: Gain ↑ x8
Minimizes background: Gain ↓ x10

IMAGINE X:

Maximizes signal: Gain ↑ x2
Minimizes background: Gain ↓ x4
Together, DNP-IMAGINE-X Gains: ↑↑x10's

Proof-of-Principle: Amplifying Hydrogen in Biological Crystals

- Prototype: x~3 gains S/N** (already comparable to Deuteration)
 - 100% negative polarization: -18.30 fm
 - 100% positive polarization: +10.82 fm
 - Dramatically enhances scattering/visibility of hydrogen
- Tunable Difference Measurements**
 - Adiabatic Fast Passage or neutron spin flipper can reverse polarization more quickly
 - Only thing that changes is the cross section for the nuclei, and that changes in a predictable manner



DNP NMC tunes the spin dependent scattering length of H_b by a near order of magnitude: A-B) Measured DNP NMC diffraction at ORNL: Spin aligned (A), Spin anti-aligned (B); C) Calculated DNP nuclear maps.

DNP-IMAGINE-X: unique capability and science

- Continuous DNP system** → 10-fold gains in S/N
- Cryogen free, superconducting 5 T Helmholtz Coil
 - ~2π Acceptance for scattered neutrons
- High power, cryogen free 1 K recirculating ⁴He refrigerator
- SiPM based anger cameras** → 5-fold gains in S/N
 - 45 cm detector distance (like MaNDi)
 - 40 cameras in 2 banks (assuming current design)
- Tunable, reversible and in situ control (~10-fold) of spin-dependent coherent scattering within a single “perfectly isomorphous” sample
- (~100 mK), high field (5 T), cold (2-10 Å) neutron Laue diffraction experiments, well matched to advanced magnetic and quantum material science
- A new, unique capability that will open and extend new fields of neutron research and discovery for the decade(s) ahead



DNP-IMAGINE-X: conceptual design of the new DNP sample environment, detector banks and upstream neutron polarization and spin-flipper system, installed at the end station of the current IMAGINE beamline

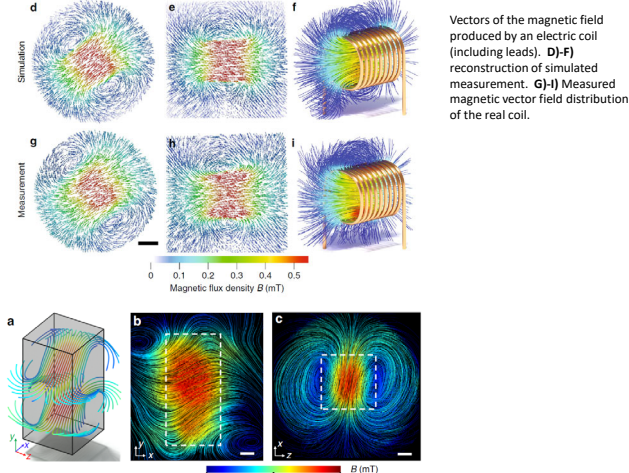
Research was performed at the HFIR and SNS, DOE Office of Science User Facilities. Parts of the research were supported by ORNL's Laboratory Directed Research and Development (LDRD) program.

Polarized Neutron applications for Materials & Engineering

2024

Longitudinal 2 Configuration (2 filters, 4 $\pi/2$ flippers) Tensor Imaging at CONRAD, HZB (V7, RIP)

Science Area	Materials & Engineering
Science Example	(1) Electric coil, (2) trapped magnetic flux within type-1 superconductor lead
Capability Family	explore magnetic scattering
Larmor	$\vec{\tau} = \vec{\mu} \times \vec{B}$, $\omega = -\gamma B$
Capability	Novel tensorial multiplicative algebraic reconstruction technique, with 9 spin polarized neutron imaging measurements
Application Statement	Quantify field magnitude and direction and domain structures, where direct probes cannot access
A. Hilger <i>et al</i> , "Tensorial neutron tomography of three-dimensional magnetic vector fields in bulk materials," <i>Nature Communications</i> 9 , 4023 (2018)	



Magnetic vector field inside a superconducting lead sample measured at $T=4.3$ K. **A)** Some selected magnetic field lines show the location of magnetic field inside the sample indicated by the cuboid. **B)** In a selected xy plane (silhouette marked by dotted lines). Scale bar, 5 mm. **C)** In a selected yz plane. Scale bar, 5 mm.

Longitudinal 1 Configuration (2 filters, 1 flipper) SANS at NCNR, NG7SANS

Science Area	Materials & Engineering
Science Example	ferromagnetic alloy $Ni_{0.89}V_{0.11}$
Capability Family	explore magnetic scattering
Capability	Isolate magnetic scattering
Application Statement	Identify small magnetic cluster contributions. Azimuthal angle dependence of spin-flip and non-spin flip scattering reveal magnetic contributions at different length scales
K. Hiroi <i>et al</i> , "Revealing magnetic correlations in ferromagnetic alloys with polarized SANS," <i>Journal of Physics, Conference Series</i> 2481 , 012001 (2023) (PNCMI)	

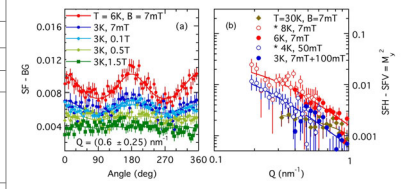


Figure 3: (a) Neutron scattering intensity (spin flip response) vs. azimuthal angle θ collected in the Q range of $(0.35-0.85)\text{nm}^{-1}$ at different temperatures T and magnetic fields B . Fits are shown as solid lines using Eq. (2). (b) Magnetic neutron scattering intensity vs. wave vector Q of the spin-flip contrast. SFISANS is shown in small magnetic fields ($B \leq 50$ mT) representing M_{iso}^2 or $1/3$ of the total isotropic magnetic response M_{iso} . *Data from lower Q range [12] are included with open symbols. Solid lines follow Eq. (4)

Half Polarized Configuration (1 filter, 1 flipper) Single crystal diffractometer at Heinz Maier-Leibnitz Zentrum, POLI

Science Area	Materials & Engineering
Science Example	ferromagnetic shape memory alloy Ni_2MnGa
Capability Family	separate nuclear and magnetic scattering
Relevant terms	$N^+N + M_{\perp}^+M_{\perp} + P \cdot M_{\perp}^+N + P \cdot M_{\perp}N^+$
Capability	separate nuclear and magnetic scattering
Application Statement	Follow moment reorientation as a function of compressive stress and magnetic field
Y.B. Ke <i>et al</i> , "Unraveling magneto-structural coupling of Ni_2MnGa alloy under the application of stress and magnetic field using in situ polarized neutron diffraction," <i>Appl. Phys. Lett.</i> 117 , 081905 (2020)	

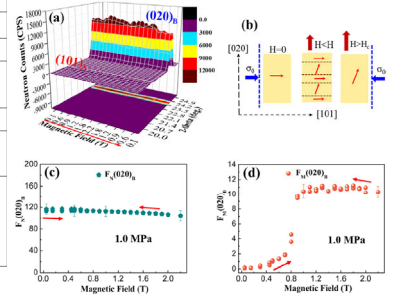
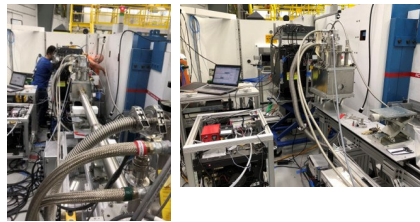
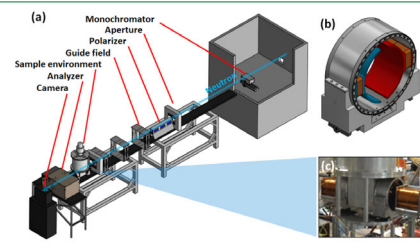
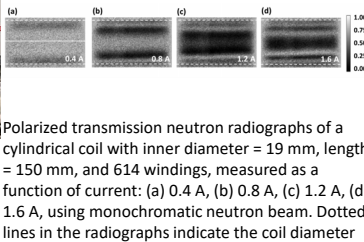


FIG. 3. (a) Change in the one-dimensional integrated peak profiles of $(101)_B$ and $(020)_B$ with spin up neutrons during the application of the magnetic field under a compressive stress of 1.0 MPa. (b) Schematic of the magnetization process driven by the magnetic field under constant stress (σ_0). Variations of (c) the nuclear structure factor F_N and (d) the magnetic structure factor F_M of the $(020)_B$ peak as a function of the magnetic field.

Longitudinal 1 Configuration (2 filters, 0 flipper, non-spin-flip only) Depolarization Imaging at MARS, HFIR CG-1D



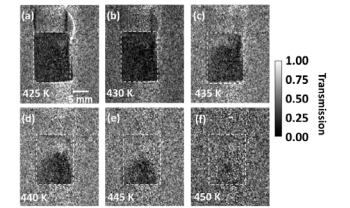
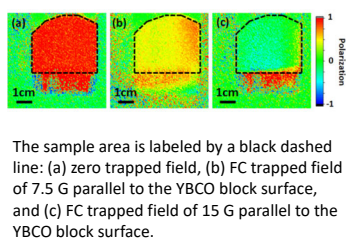
Sc. A. Materials & Engineering	Sc. A. Materials & Engineering	Sc. A. Materials & Engineering
Sc. Ex. Cylindrical coil at varying current	Sc. Ex. Single crystal of superconductor $YBa_2Cu_3O_7$	Sc. Ex. Ferromagnetic powder Fe_3Pt
Cap. Fam. Explore Magnetism	Cap. Fam. Explore Magnetism	Cap. Fam. Explore Magnetism
Larmor $\vec{\tau} = \vec{\mu} \times \vec{B}$, $\omega = -\gamma B$		
Cap. Depolarization of transmitted beam	M-B $(P \cdot M_{\perp}^+)M_{\perp} + (P \cdot M_{\perp})M_{\perp}^+ - P(M_{\perp}^+M_{\perp})$	M-B $(P \cdot M_{\perp}^+)M_{\perp} + (P \cdot M_{\perp})M_{\perp}^+ - P(M_{\perp}^+M_{\perp})$
App. St. Observe depolarization effects of electromagnet as a function of position and current	Cap. Depolarization of transmitted beam	Cap. Depolarization of transmitted beam
	App. St. Observe trapped fields within superconductor	App. St. Observe transition from ferromagnetic to paramagnetic state through T_c
I. Dhiman <i>et al</i> , <i>Rev. Sci. Instrum.</i> 88 095103 (2017)	T. Wang <i>et al</i> , <i>Rev. Sci. Instrum.</i> 90 033705 (2019)	I. Dhiman <i>et al</i> , <i>Rev. Sci. Instrum.</i> 88 095103 (2017)



Polarized transmission neutron radiographs of a cylindrical coil with inner diameter = 19 mm, length = 150 mm, and 614 windings, measured as a function of current: (a) 0.4 A, (b) 0.8 A, (c) 1.2 A, (d) 1.6 A, using monochromatic neutron beam. Dotted lines in the radiographs indicate the coil diameter

The sample area is labeled by a black dashed line: (a) zero trapped field, (b) FC trapped field of 7.5 G parallel to the YBCO block surface, and (c) FC trapped field of 15 G parallel to the YBCO block surface.

Polarized neutron radiographs for Fe_3Pt ($10 \times 3 \times 20$ mm 3) as a function of temperature, with an exposure time of 600 s: (a) 425 K, (b) 430 K, (c) 435 K, (d) 440 K, (e) 445 K, (f) 450 K. Measurements are carried out while heating the sample from 425 K to 450 K. White dashed boxes show the sample area. Contrast of the radiographs is enhanced artificially to improve the visualization of magnetic effects inside the sample.

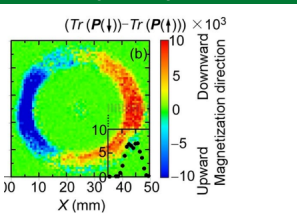


Plans for more polarized imaging at both MARS & VENUS (SNS, BL-10)

Depolarization Imaging at J-PARC, RADEN (BL22)

Science Area	Materials & Engineering
Science Example	Inductor with Mn-Zn ferrite core
Capability Family	explore magnetic scattering
Larmor	$\vec{\tau} = \vec{\mu} \times \vec{B}$, $\omega = -\gamma B$
Capability	Depolarization
Application Statement	Quantify field magnitude and direction within the ferrite core of an inductor, where direct probes cannot access

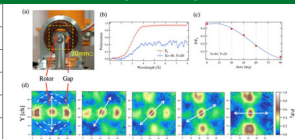
H. Mamiya *et al*, "Neutron imaging for magnetization inside an operating inductor," *Scientific Reports* **13**, 9184 (2023)



Depolarization Imaging at J-PARC, NOBORU (BL10)

Science Area	Materials & Engineering
Science Example	Electric motor
Capability Family	explore magnetic scattering
Larmor	$\vec{\tau} = \vec{\mu} \times \vec{B}$, $\omega = -\gamma B$
Capability	Depolarization
Application Statement	Quantify field magnitude and direction within an electric motor, where direct probes cannot access

K. Hiroi *et al*, "Magnetic field imaging of a model electric motor using polarized pulsed neutrons at J-PARC/MLF," *Journal of Physics, Conference Series* **862**, 012008 (2017) (PNCMI)

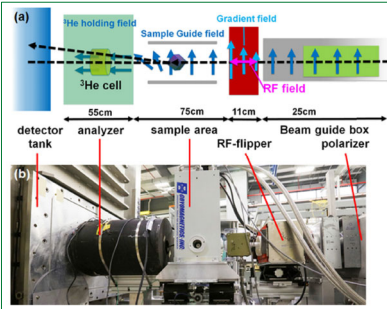


We're just getting started: Emerging polarized neutron configurations on fresh instruments

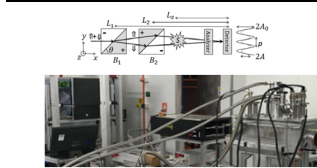
2024

L. Debeer-Schmitt, H. Bilheux, Y. Zhang, M. Frontzek, C.Y. Jiang, L. Crow, F. Li

Polarized neutrons enable a variety of capabilities which enhance 'unpolarized' neutron scattering techniques by separating different aspects and dimensions of scattering, or providing high resolution in energy and/or angle. At ORNL, we are expanding the utility of polarized neutron scattering to more neutron scattering techniques, enabling a more nuanced understanding of the systems under study.



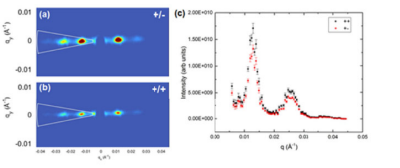
SEMSANS, ORNL prisms @ ISIS



Upgrade planned for GP-SANS for more routine configuration changes

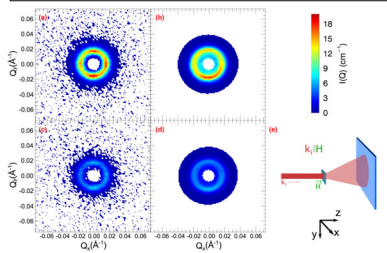
Small Angle Neutron Scattering at GP-SANS, HFIR CG-2

Longitudinal 1 Configuration (2 filters 1 flipper, spin-flip and non-spin-flip only)	
Science Area	Condensed matter
Science Example	Single crystal of helical magnet $\text{Cr}_{1/3}\text{NbS}_2$
Capability Family	Explore Magnetism
Relevant M-B terms	$(P \cdot M_{\parallel}^{\uparrow})M_{\perp} + (P \cdot M_{\perp})M_{\parallel}^{\uparrow} - P(M_{\parallel}^{\uparrow}M_{\perp})$
Capability	Compare M_{\perp} to M_{\parallel}
Application Statement	Quantify ellipticity of chiral structure
T. Wang et al, <i>Physica B</i> 551 492 (2018)	



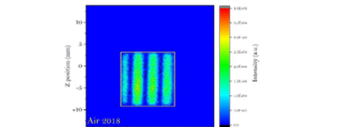
(a) Raw 2D scattering data of the +/- spin state of the helical magnets $\text{Cr}_{1/3}\text{NbS}_2$ (b) Raw 2D scattering data of the +/- spin state of the helical magnets $\text{Cr}_{1/3}\text{NbS}_2$ (c) Peaks represent helical periodicity. Comparison between the two spin configurations of the azimuthal integrated scattering cross section as a function of Q after the effect of the ^3He decay has been taken into consideration

Half Polarized Configuration (1 filter 1 flipper, intensity variations only)	
Sc. A.	Condensed matter
Sc. Ex.	Nanopillars of ferromagnetic CoFe_2O_4 in ferroelectric BaTiO_3
Cap. Fam.	Explore Magnetism
M-B	$P \cdot M_{\perp}^{\uparrow}N + P \cdot M_{\perp}N^{\uparrow}$
Cap.	Difference is predominantly a measure of M_{\perp}
App. St.	Compare to nano-pillar model to distinguish and locate 2 magnetic phases in nanopillars
T.O. Farmer et al, <i>Phys. Rev. Mat.</i> 3 081401(R) (2019)	

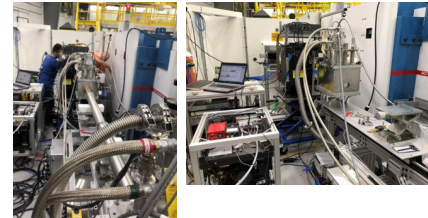
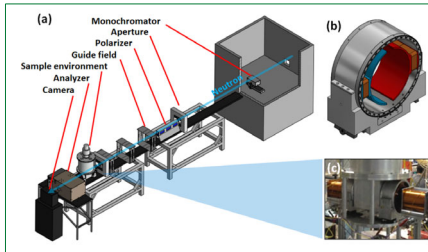


SANS with polarized neutron beam for +7 mT and model fit: (a),(b) I+Q, (c),(d) I-Q. The ring feature is identified at $Q = 0.0168 \text{ \AA}^{-1}$. (e) Schematic of neutron experiment. The final wave vector k_f lies inside the cone. The scattering vector Q lies in the green colored plane at the position of the sample. Pillars parallel to the incident beam and the neutron beam polarization. Samples were saturated with a +7 T out-of-plane field ex situ and then measured at +7 mT (near remanence) and -500 mT field where the sign is taken with respect to the saturation field

Larmor Configuration (2 filter 2 Wollaston Prisms)	
Sc. A.	Materials & Engineering
Sc. Ex.	Mesoporous silica forming over time
Cap. Fam.	Enhance resolution
Larmor	$\vec{\tau} = \vec{\mu} \times \vec{B}, \omega = -\gamma B$
Cap.	Up to 2.5 μm sensitivity via enhanced angle resolution
App. St.	Observe simultaneous emergence of large particles and Bragg peaks
J. Schmitt et al, <i>ACS Appl. Mater. Interfaces</i> 12 28461 (2020)	
F. Li et al, <i>Sci Rep</i> 9 8563 (2019)	



Intensity modulation of one of the spin states with air being the blank. The wavelength of this frame is 6.27 Å. The yellow box indicates the area of interest used to calculate Γ



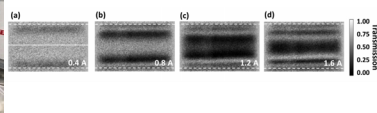
Plans for more polarized imaging at both MARS & VENUS (SNS, BL-10)

Longitudinal 1 Configuration (2 filters, 0 flipper, non-spin-flip only) Depolarization Imaging at MARS, HFIR CG-1D

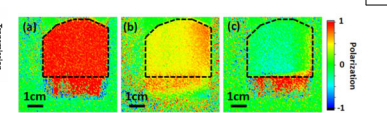
Sc. A.	Condensed matter
Sc. Ex.	Cylindrical coil at varying current
Cap. Fam.	Explore Magnetism
Larmor	$\vec{\tau} = \vec{\mu} \times \vec{B}, \omega = -\gamma B$
Cap.	Depolarization of transmitted beam
App. St.	Observe depolarization effects of electromagnet as a function of position and current
I. Dhiman et al, <i>Rev. Sci. Instrum.</i> 88 095103 (2017)	

Sc. A.	Condensed matter
Sc. Ex.	Single crystal of superconductor $\text{YBa}_2\text{Cu}_3\text{O}_7$
Cap. Fam.	Explore Magnetism
M-B	$(P \cdot M_{\parallel}^{\uparrow})M_{\perp} + (P \cdot M_{\perp})M_{\parallel}^{\uparrow} - P(M_{\parallel}^{\uparrow}M_{\perp})$
Cap.	Depolarization of transmitted beam
App. St.	Observe trapped fields within superconductor
T. Wang et al, <i>Rev. Sci. Instrum.</i> 90 033705 (2019)	

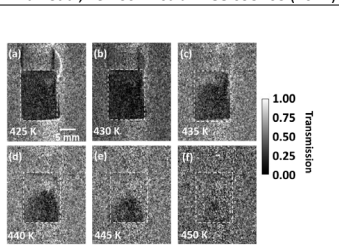
Sc. A.	Condensed matter
Sc. Ex.	Ferromagnetic powder Fe_3Pt
Cap. Fam.	Explore Magnetism
M-B	$(P \cdot M_{\parallel}^{\uparrow})M_{\perp} + (P \cdot M_{\perp})M_{\parallel}^{\uparrow} - P(M_{\parallel}^{\uparrow}M_{\perp})$
Cap.	Depolarization of transmitted beam
App. St.	Observe transition from ferromagnetic to paramagnetic state through T_c
I. Dhiman et al, <i>Rev. Sci. Instrum.</i> 88 095103 (2017)	



Polarized transmission neutron radiographs of a cylindrical coil with inner diameter = 19 mm, length = 150 mm, and 614 windings, measured as a function of current: (a) 0.4 A, (b) 0.8 A, (c) 1.2 A, (d) 1.6 A, using monochromatic neutron beam. Dotted lines in the radiographs indicate the coil diameter



The sample area is labeled by a black dashed line: (a) zero trapped field, (b) FC trapped field of 7.5 G parallel to the YBCO block surface, and (c) FC trapped field of 15 G parallel to the YBCO block surface.

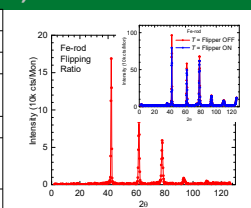


Polarized neutron radiographs for Fe_3Pt ($10 \times 3 \times 20 \text{ mm}^3$) as a function of temperature, with an exposure time of 600 s: (a) 425 K, (b) 430 K, (c) 435 K, (d) 440 K, (e) 445 K, (f) 450 K. Measurements are carried out while heating the sample from 425 K to 450 K. White dashed boxes show the sample area. Contrast of the radiographs is enhanced artificially to improve the visualization of magnetic effects inside the sample.



Half-Polarized Configuration (1 filter, 1 flipper, changes in scattered intensity only) Powder Diffraction at WAND², HFIR HB-2C

Science Area	Condensed matter
Science Example	Polycrystalline ferromagnet Fe
Capability Family	Explore Magnetism
Relevant M-B terms	$P \cdot M_{\perp}^{\uparrow}N + P \cdot M_{\perp}N^{\uparrow}$
Capability	Determine magnetization density
Application Statement	Initial demonstration, magnetization density in room temperature Fe rod
unpublished; early demonstration	



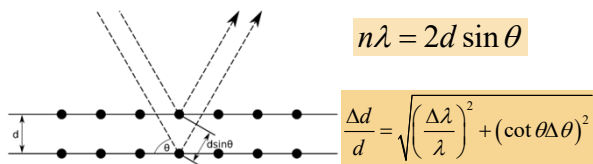
Configurations to enhance contrast access either changes in scattered neutron **intensity** and/or **polarization state**.
Capabilities access specific contributions to these changes, either as found in the Maleev-Blume equations, via Larmor precession of the neutrons, or via changes in absorption.
Configurations to enhance resolution leverage Larmor precession **before and/or after the sample.**

High resolution boosted by Larmor labeling of neutron spin

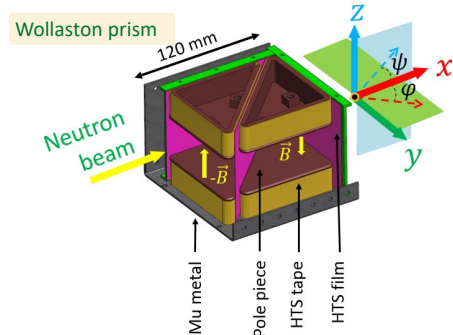
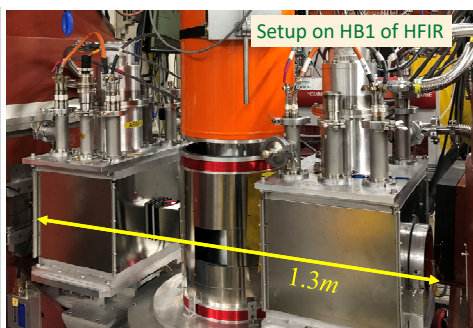
Fankang Li¹, K. Burrage¹, F. Funama¹, L. Crow¹, M. Matsuda², K. Hong³, M. Manley⁴, R. Hermann⁴, O. Delaire⁵

1. Neutron Technologies Division, ORNL. 2. Neutron Scattering Division, ORNL. 3. Center for Nanophase Materials Sciences, ORNL. 4. Materials Science and Technology Division, ORNL. 5. Mechanical Engineering and Materials Science, Duke University.

Conventional diffractometer



- > Resolution limited by the beam divergence and wavelength spread
- > Typical resolution is $\Delta d/d = 10^{-2} - 10^{-3}$

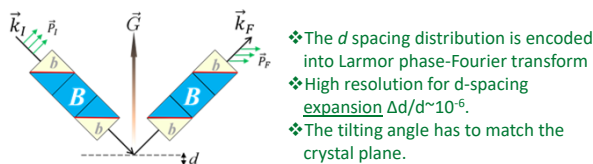


Principle of Larmor diffraction

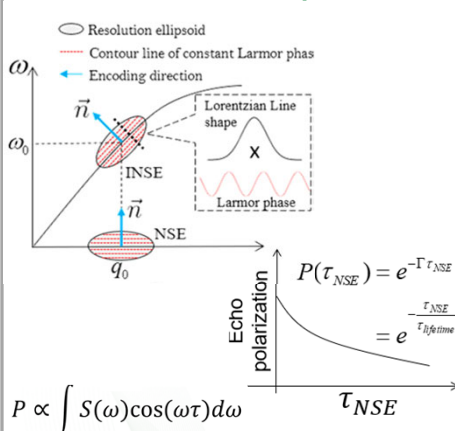
Bragg's Law: $k_{i,\perp} = \frac{2\pi}{d}$

Larmor phase: $\Phi = \frac{\gamma_N m B L d}{\hbar k_{i,\perp}}$

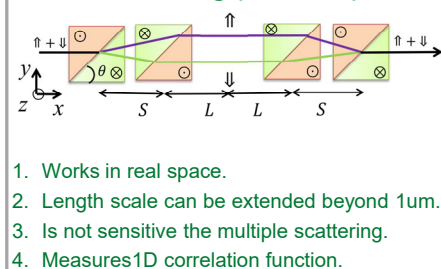
$\Phi = \frac{\gamma_N m B L d}{2\pi \hbar}$



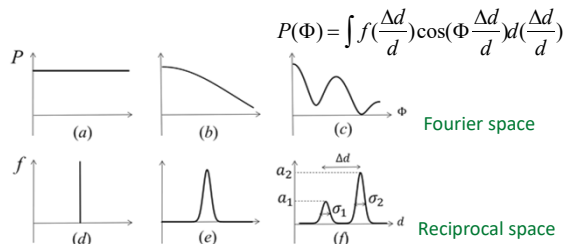
Inelastic Neutron Spin Echo



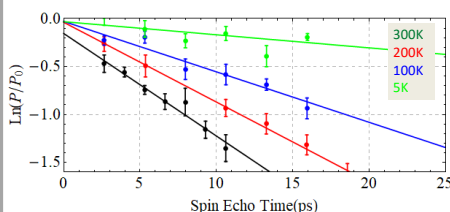
Spin Echo Small Angle Neutron Scattering (SESANS)



Data interpretation-a Fourier transform



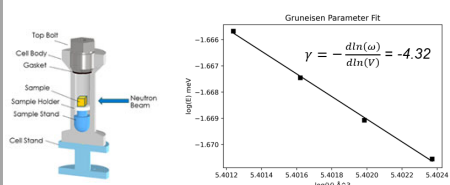
Phonon lifetime of Bismuth



Temperature(K)	Linewidth from simulation (μ eV)	Linewidth from HB1 (μ eV)
100	15	25.65 \pm 7.06
200	32	45.79 \pm 3.57
300	52.5	61.41 \pm 7.86

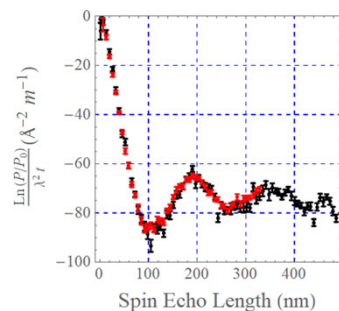
An energy resolution of $<10\mu$ eV has been achieved to measure both the phonon energy shift and linewidth of Bismuth

Grüneisen Parameter Measurement of GaSb

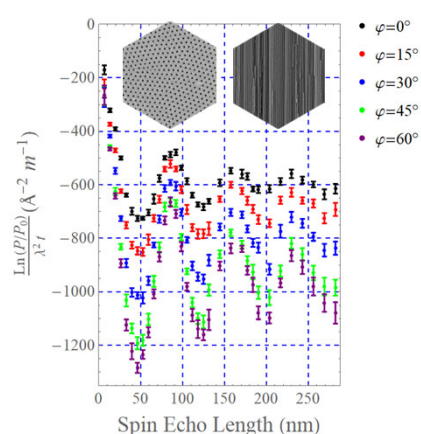


Capable of measuring the Grüneisen parameter with large sample (8 cm³) and low pressure (1kbar) due to the high energy resolution of INSE.

35% Polymethyl methacrylate (PMMA)



Nanoporous alumina



References

- Li, F. et al., (2017). *Scientific Reports* **7**, 865.
- Li, F. et al., (2014). *Rev. Sci. Instrum.* **85**, 053303.
- Li, F. et al., (2014). *J. Appl. Cryst.* **47**, 1849-1854.
- Li, F. et al., (2018). *J. Appl. Cryst.* **51**, 584-590
- Please visit: <https://fankangli.ornl.gov/>